

Lu-Hf garnet geochronology of eclogites from the Balma Unit (Pennine Alps): implications for Alpine paleotectonic reconstructions

DANIEL HERWARTZ^{1,*}, CARSTEN MÜNKER^{1,2}, ERIK E. SCHERER², THORSTEN J. NAGEL¹, JAN PLEUGER¹ & NIKOLAUS FROITZHEIM¹

Key words: Lu-Hf geochronology, Western Alps, Balma Unit, Monte Rosa, tectonic evolution

ABSTRACT

Three samples of eclogite from the Balma Unit, an ophiolite sheet on top of the Monte Rosa Nappe in the Pennine Alps, were investigated in terms of their P-T evolution, geochemistry, and Lu-Hf geochronology. The paleogeographic origin of this unit is controversial (North Penninic vs. South Penninic). It has been interpreted as a piece of Late Cretaceous oceanic crust, on the basis of ca. 93 Ma U-Pb SHRIMP ages of synmagmatic zircon cores in an eclogite. Trace element and isotope data suggest a mid ocean ridge (MOR) rather than an intraplate or OIB setting for the protoliths of the eclogites. Electron microprobe analyses of representative garnets show typical prograde zoning profiles. Estimated peak metamorphic temperatures of 550–600 °C most likely did not exceed the closure temperature of the Lu-Hf system. Hence, Lu-Hf ages most likely reflect garnet growth in the studied samples. To minimize inclusion effects on age determinations, a selective digestion procedure for garnet was applied, in which zircon and rutile inclusions are not dissolved. The ages obtained for three samples, 42.3 ± 0.6 Ma (MSWD: 0.47), 42 ± 1 Ma

(MSWD: 3.0) and 45.5 ± 0.3 Ma (MSWD: 0.33), are younger than all Lu-Hf ages reported so far for South Penninic Units. Metamorphic zircon domains of the 42.3 Ma sample (PIS1) were previously dated by U-Pb SHRIMP at 40.4 ± 0.7 Ma, indicating that the growth of metamorphic zircon post-dated the onset of garnet growth.

These new data put important constraints on the paleogeographic reconstruction of the Alps. The MORB character of the rocks, together with their previously published protolith age, imply that oceanic spreading was still taking place in the Late Cretaceous. This supports a North Penninic origin for our samples because plate tectonic models predict Cretaceous spreading in the North Penninic but not in the South Penninic Ocean. If the Balma Unit is indeed North Penninic, the new Lu-Hf data, in combination with published geochronological data, require that two independent subduction zones consumed the South and North Penninic oceans.

1. Introduction

Despite a wealth of geological and geochronological data, there are still conflicting models for the tectonic evolution of the Alps. Current rapid progress in dating metamorphic minerals such as garnet has provided a new tool to date tectono-metamorphic events in high pressure terrains. In this study, we apply Lu-Hf garnet geochronology to high-pressure rocks of the Balma Unit in the Swiss-Italian Pennine Alps. This area is formed by a stack of nappes, the Penninic Nappes (Figs. 1, 2), which originate partly from continental crust (Variscan basement with Permian and Mesozoic cover rocks), and partly from Mesozoic oceanic crust. These rocks were imbricated from the latest Cretaceous through the Early Tertiary and affected by several phases of folding and shearing. This modified the initial geometry of the nappes to such an extent that restoring the deformation back to the pre-orogenic arrangement of the units is difficult and controversial.

Most authors agree that in the Cretaceous, two partly oceanic basins existed between Europe to the Northwest and Adria (Apulia) to the Southeast: the South Penninic or Piemont-Ligurian Ocean, and the North Penninic or Valais Ocean. The former opened in the Middle and Late Jurassic, and the latter opened in the Cretaceous (Stampfli et al. 1998). The Briançonnais continental peninsula represented an eastward-tapering promontory of the Iberian continent between these two oceanic basins (Frisch 1979; Stampfli 1993). Due to the sinistrally transtensive opening of the North Penninic Ocean along a trace oblique to the South Penninic Ocean, Jurassic crust of the South Penninic Ocean was captured in the North Penninic basin, in addition to the new, Cretaceous-age oceanic crust (Fig. 2b; Liati et al. 2005).

Continental crustal rocks of the Sesia and Dent Blanche nappes occupy the highest position in the nappe stack. They originated – according to an interpretation preferred by the present authors – from a continental fragment in the South

¹ Steinmann-Institut, Universität Bonn, Germany. E-mail: danielherwartz@gmx.de

² Institut für Mineralogie, Universität Münster, Germany.

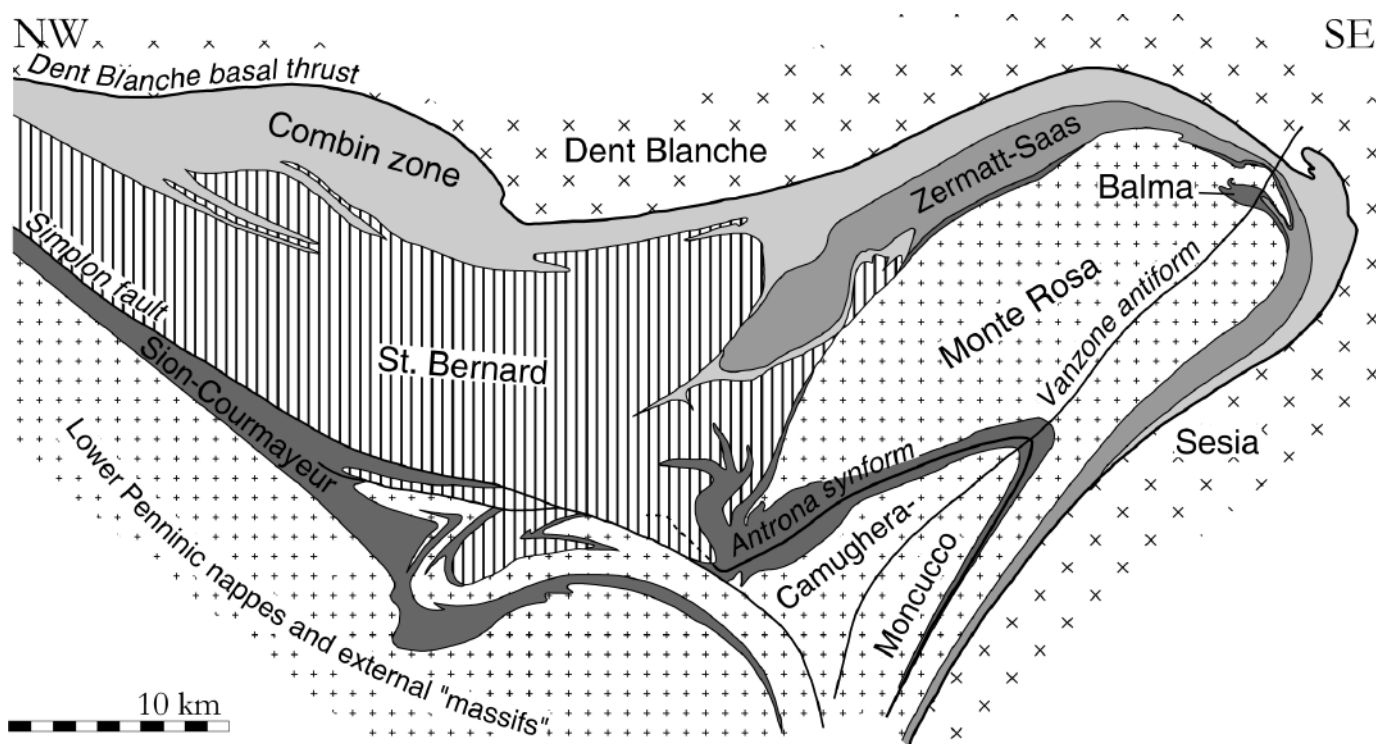


Fig. 1. Cross section through the Swiss–Italian Western Alps, modified after Escher et al. (1993). In this profile and in Fig. 2a, small crosses indicate former European continental crust, dark grey North Penninic ophiolites, vertical ruling Briançonnais continental crust, middle grey South Penninic ophiolites from the Zermatt-Saas Basin, light grey South Penninic ophiolites from the Tsaté Basin, and “x” pattern units from the Cervinia continental fragment. The paleogeographic affiliation shown here follows the interpretation of Froitzheim (2001) and Pleuger et al. (2007).

Penninic Ocean, called the Margna-Sesia fragment or Cervinia (Froitzheim & Manatschal 1996; Froitzheim et al. 1996; Schmid et al. 2004; Pleuger et al. 2007). According to other workers, these nappes were derived from the Adriatic continental margin proper (Stampfli 1993; Avigad et al. 1993). Ophiolite units occur below the Dent Blanche-Sesia nappe system. These are subdivided into two large units, the structurally higher Combin Zone and the structurally deeper Zermatt-Saas Zone. The Combin Zone records lower pressures during the subduction-related metamorphism (blueschist facies; Bousquet et al. 2004) than the Zermatt-Saas Zone (eclogite facies, locally with coesite; Reinecke 1991, 1998; Bousquet et al. 2004).

The eclogite-facies ophiolites of the Zermatt-Saas Zone overlie continental basement rocks of the Monte Rosa Nappe. The latter include paragneisses, Late Variscan to post-Variscan granites partly transformed to orthogneisses, and amphibolite boudins that in some places contain eclogite relics. In the area under consideration, on the southern flank of the Monte Rosa massif, the ophiolites of the Zermatt-Saas Zone do not rest directly on the Monte Rosa gneisses, but on a thin layer of gneiss (Stolemburg Unit), which overlies an ophiolite layer (Balma Unit), which in turn rests on the Monte Rosa Nappe (Pleuger et al. 2005). This geometry is modified by three phases of folding postdating the emplacement of the nappes (Figs. 3, 4). The Balma Unit is made up mostly of serpentinite, eclogite,

and minor amphibolite. The paleogeographic origins of these units are controversial. According to Froitzheim (2001); Liati & Froitzheim (2006), and Pleuger et al. (2005, 2007), the Monte Rosa Nappe represents the European continental margin, the overlying Balma Unit the North Penninic Ocean, the Stolemburg Unit the Briançonnais, and the rest of the Zermatt-Saas Zone the South Penninic Ocean. According to other authors (Keller & Schmid 2001; Kramer et al. 2003), the Monte Rosa Nappe originates from the Briançonnais continental crust and the overlying units (Balma, Stolemburg, Zermatt-Saas) all represent the South Penninic Ocean. These controversial views result from different ways of retrodeforming the complex geometry of the Penninic nappes.

Eclogite from the Balma Unit (sample PIS1) has recently been the subject of U-Pb SHRIMP geochronology on zircon (Liati & Froitzheim 2006). Magmatic zircon domains yielded a Cretaceous protolith age of 93.4 ± 1.7 Ma (Cenomanian-Turonian) and metamorphic domains a Late Eocene age of 40.4 ± 0.7 Ma, interpreted as the age of high-pressure metamorphism. In the present study, we studied the geochemistry, P-T evolution, and Lu-Hf geochronology of the same sample PIS1 and two other eclogites from the Balma Unit to put additional constraints on the origin and metamorphic history of these rocks.

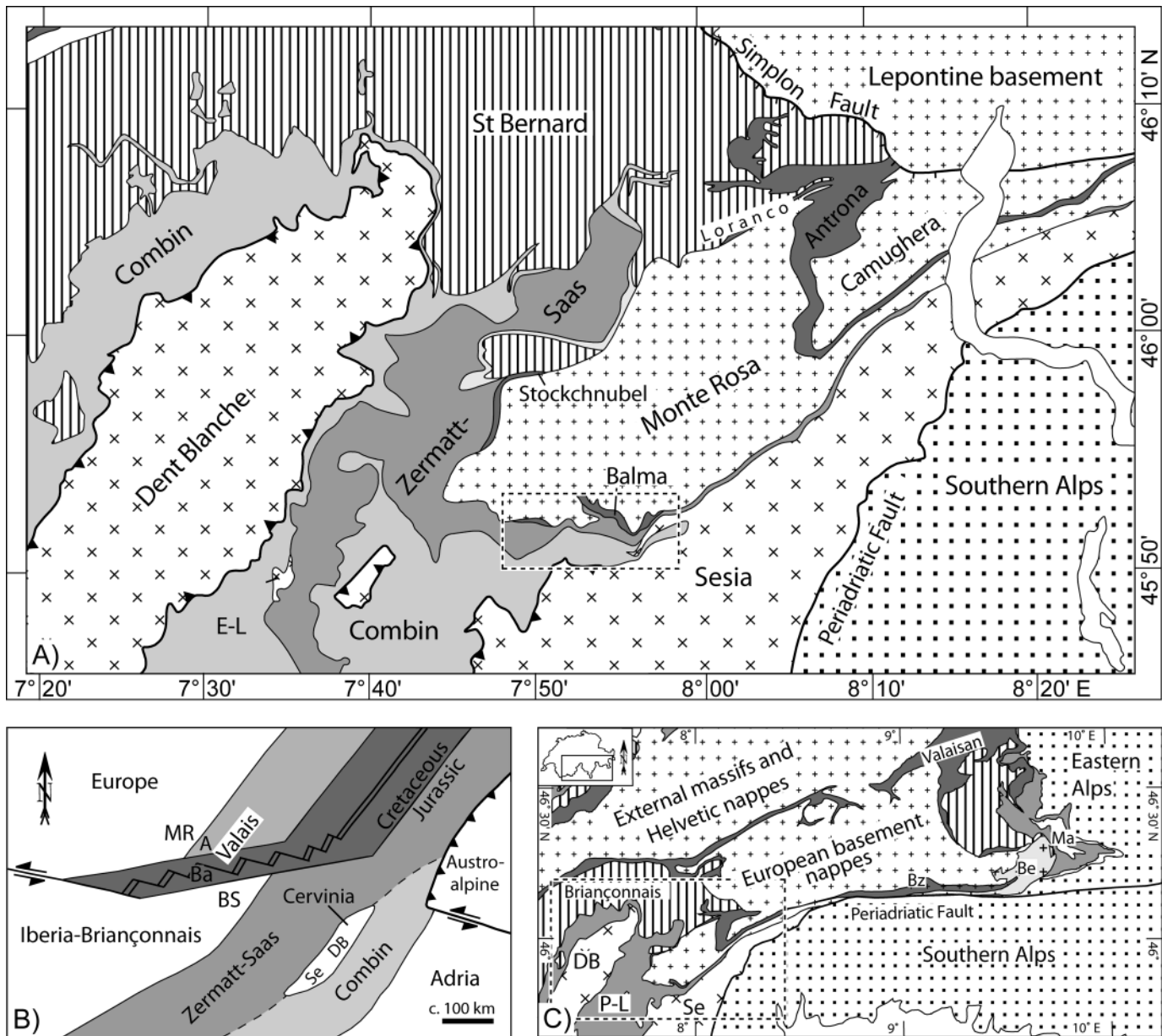


Fig. 2. (A) Tectonic map of the Penninic nappe stack between the Sesia-Dent-Blanche nappe system and the Simplon line, modified after Steck et al. (1999). E-L Etiroi-Levaz sliver. (B) Paleogeographical sketch map of continental and oceanic domains for early Late Cretaceous time. MR Monte Rosa, A Antrona, Ba Balma, BS St. Bernard and Stolemberg, DB Dent-Blanche, Se Sesia. (C) Overview map of the Central Alps. Bz Bellinzona-Dascio Zone, Be Bergell Pluton, Ma Margna Nappe, P-L Piemont-Ligurian (South Penninic) ophiolites.

2. Sample description, petrography and P-T evolution

Three partially retrogressed eclogites, all sampled close to Alpe la Balma, NW of Alagna Valsesia (Figs. 3 and 4), have been investigated in detail. All three eclogites contain garnet, amphibole, clinozoisite, quartz, paragonite, albite, and rutile \pm epidote, \pm chlorite, \pm zircon and \pm opaques. Sample MR56 also displays a small amount of phengite allowing the application of the Grt-Cpx-Phg barometer (Ravna & Terry 2004). Although there is a weak retrograde overprint, the peak-pressure assemblage (Grt

+ Cpx1 + Pg Qtz + Rt + Am1 \pm Phg) is well preserved in all samples investigated (Fig. 5).

Garnets are usually 0.5–3 mm in diameter and euhedral. They often have inclusions in their cores and wide, almost inclusion-free rims (Fig. 5a). Inclusions in garnet comprise clinopyroxene, amphibole, quartz, clinozoisite, rutile, sphene. There are also rare plagioclase inclusions, but it is not clear whether these are primary or products of retrograde reactions. Garnets display typical prograde compositional patterns with elevated grossular and spessartine components in the cores and a bell-

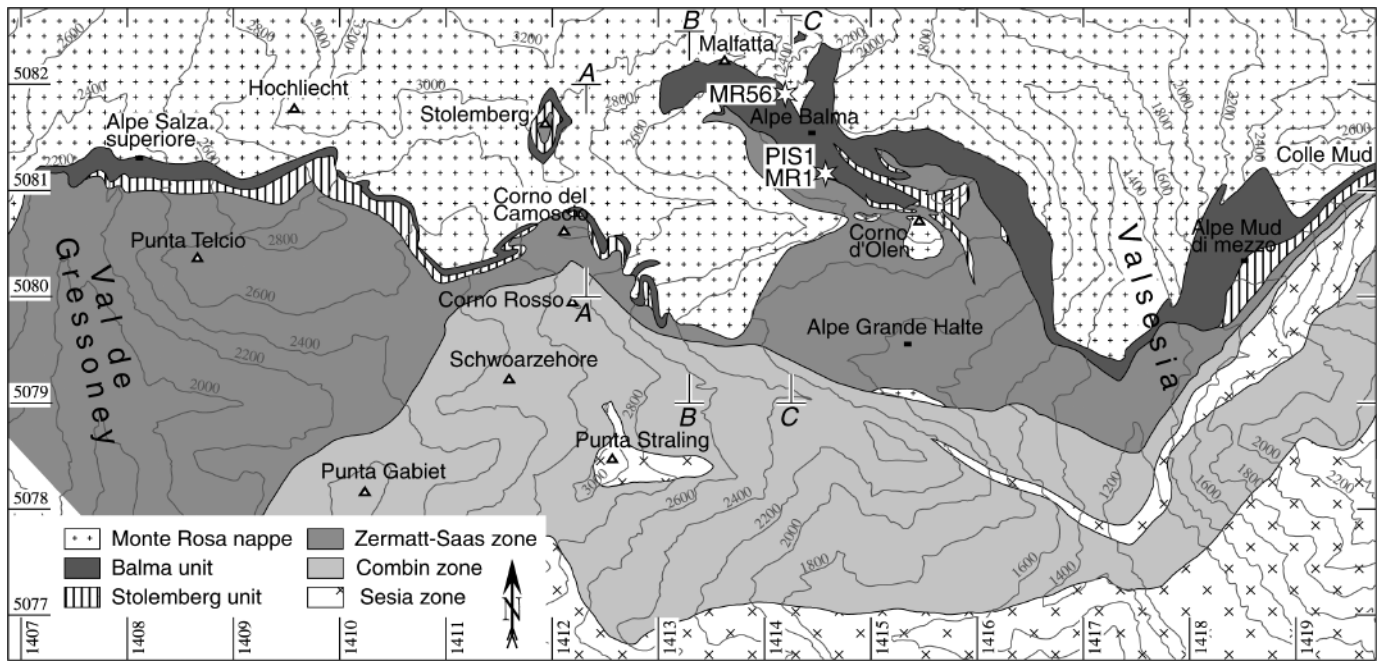


Fig. 3. Geological map of the upper Sesia and Gressoney valleys. Italian Gauss-Boaga coordinates for sample locations are E:1414610 N:5081110 for samples PIS1 and MR1 collected at the same outcrop and R:1414270 H:5081930 for sample MR56. ZS = Zermatt-Saas, MR = Monte-Rosa, white stars = sample locations. The map area is marked by the rectangle in Figure 2 (top).

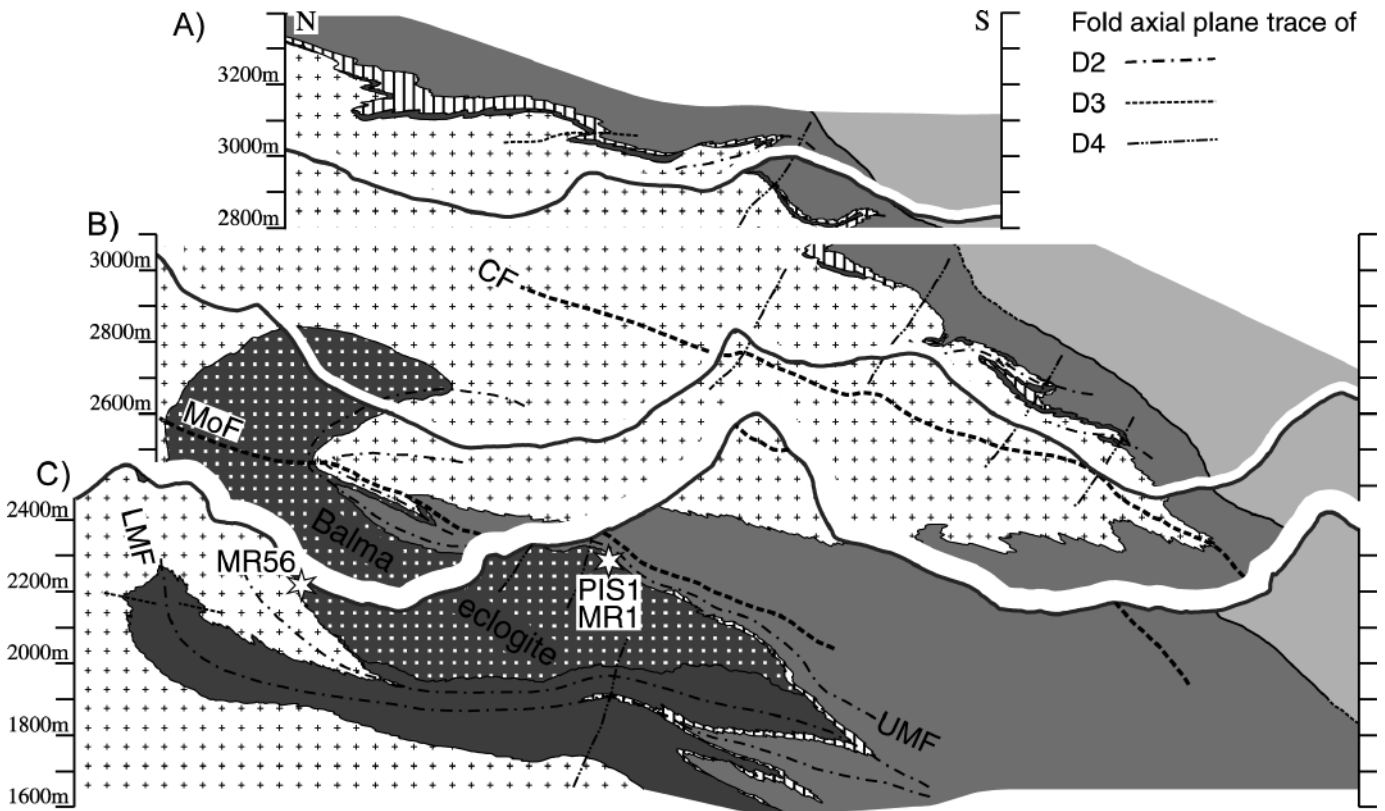


Fig. 4. Tectonic interpretation of north-south cross sections through the study area. Positions of the sections are indicated in Figure 3. CF: Axial trace of the Cimalegna Fold; LMF: Lower Malfatta Fold; MoF: Molera Fold; UMF: Upper Malfatta Fold

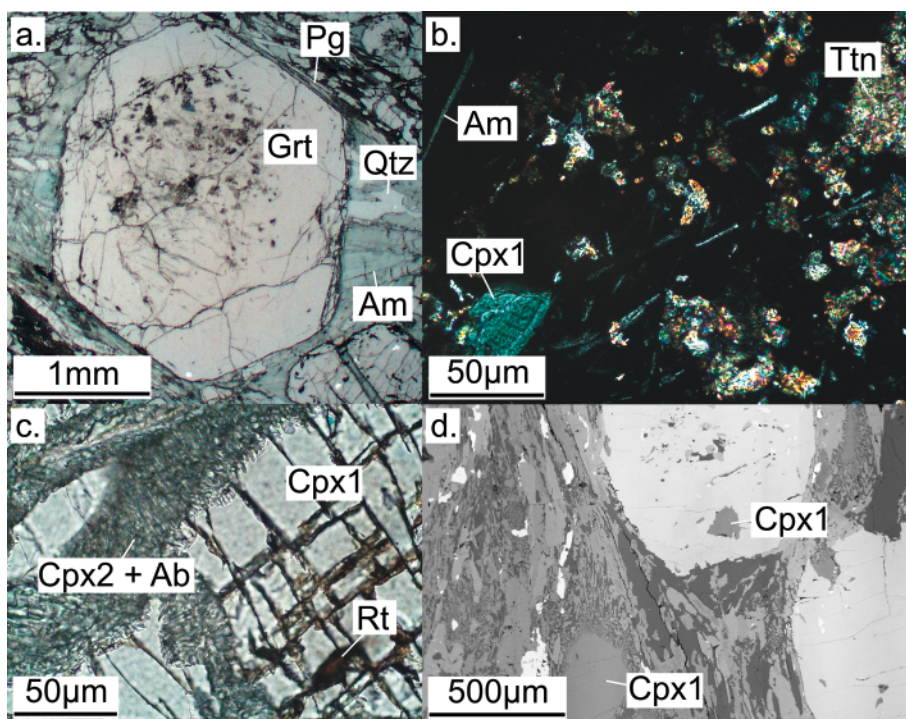


Fig. 5. Thin sections (a,b,c) and BSE image (d) of the studied samples. (a) Large idiomorphic garnet (sample MR1) with a typically inclusion-rich core and an almost inclusion-free rim. (b) Enlarged image of the garnet core from image a, with inclusions of titanite, amphibole, and sodium rich clinopyroxene (Cpx1). (c) Symplectite of albite and sodium-poor clinopyroxene (Cpx2), which grew at the expense of Cpx1 (MR56). (d) BSE image of sample MR56. Inclusions of clinopyroxene in garnet are sodium-rich Cpx1. Mineral abbreviations are after Kretz (1983), except: Am = amphibole.

shaped distribution of the $Fe/(Fe+Mg)$ ratio (Fig. 6). Chemical profiles across the garnets and X-ray mapping confirm the petrographic observation that there is little or no corrosion or retrograde re-equilibration of garnets because in most cases neither the spessartine component nor the $Fe/(Fe+Mg)$ show an increase towards the very rim. However, garnet cores can occasionally be completely retrogressed, with the rim still being intact. Two generations of clinopyroxene are present (Table 1). Matrix clinopyroxene (Cpx1) is extremely sodium-rich with X_{Na} in excess of 0.5 in all samples reflecting the high sodium contents of the bulk rocks. Clinopyroxene 1 is often rimmed by symplectites of fine-grained albite and sodium-poor clinopyroxene (Cpx2). In samples MR1 and PIS1, only a few crystals of amphibole and clinozoisite are visible in thin section. Together with elongated domains of symplectite around Cpx1, these two minerals define a weak foliation. In contrast, sample MR56 was more strongly deformed during retrogression, the formation of symplectites is more pronounced, and there is abundant clinozoisite, which is well-aligned in shear bands and along the main foliation. Amphibole generally has a high glaucophane component (Am1: SiO_2 content of 52–55 wt%; Na mainly on the B-site). Occasionally, they have thin rims of barroisitic/pargasitic hornblende (Am2: SiO_2 content of 40–42 wt%; Na mainly on the A-site). Feldspar is only present in symplectites and is generally pure albite. Phengite in sample MR56 contains about 6.8 p.f.u. of Si. We only found a couple of grains but these were sub- to euhedral and appear to have been in equilibrium with the high pressure assemblage. In contrast to phengite, large paragonite crystals are abundant in all samples.

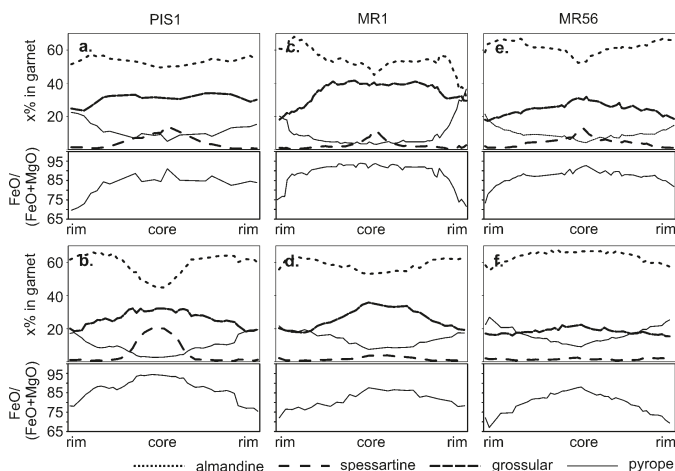


Fig. 6. Element profiles plotted for selected garnet grains from samples PIS1 (a,b), MR1 (c,d) and MR56 (e,f). Garnets were selected by their high Mn count rates obtained from element mapping, implying that the grains were cut close to their cores. Garnet grain diameters are (a) 1 mm, (b) 1.2 mm, (c) 3 mm, (d) 0.8 mm, (e) 2.5 mm and (f) 2 mm.

Pressures obtained with the Grt-Cpx-Phg barometer (Ravna & Terry 2004) for sample MR56 range from 17 to 20 kbar (at temperatures between 400 and 700 °C; Fig. 7). Various Grt-Cpx thermometers yielded a wide range of unreasonably low temperatures (200–450 °C). To constrain the P-T evolution, we calculated an equilibrium phase diagram (De Capitani 1994) for a simplified bulk composition of sample MR56 (Si-Al-Fe-

Table 1. Representative microprobe analyses of eclogite phases in wt% and p.f.u. *All Fe is calculated as FeO.

| Sample: Mineral: | MR56 Grt (rim) | MR56 Grt (core) | MR56 Cpx 1 | MR56 Am 1 | MR56 Am 2 | MR56 Ab | MR56 Pg | MR1 Grt (rim) | MR1 Grt (core) | MR1 Cpx 1 | MR1 Cpx 2 | MR1 Ab | PIS1 Grt (rim) | PIS1 Grt (core) |
|--------------------------------|----------------------|-----------------------|---------------|--------------|--------------|------------|------------|---------------------|----------------------|--------------|--------------|-----------|----------------------|-----------------------|
| SiO ₂ | 37.9 | 37.5 | 55.5 | 53.7 | 40.4 | 67.4 | 51.1 | 38.9 | 39.3 | 56.3 | 53.3 | 67.4 | 38.3 | 38.3 |
| TiO ₂ | 0.073 | 0.152 | 0.033 | 0.135 | 0.032 | <DL | 0.175 | 0.072 | 0.191 | 0.024 | 0.093 | 0.002 | 0.051 | 0.103 |
| Al ₂ O ₃ | 21.8 | 21.6 | 10.5 | 7.02 | 18.1 | 19.7 | 27.7 | 22.1 | 22.0 | 11.8 | 1.85 | 20.0 | 22.2 | 22.1 |
| FeO* | 29.6 | 28.1 | 6.18 | 7.83 | 14.9 | 0.178 | 1.63 | 29.3 | 19.9 | 3.32 | 5.85 | 0.234 | 28.8 | 19.4 |
| MnO | 0.404 | 1.37 | 0.041 | 0.093 | 0.183 | <DL | 0.012 | 0.155 | 4.96 | <DL | 0.163 | <DL | 0.610 | 8.57 |
| MgO | 3.89 | 2.21 | 7.31 | 16.3 | 9.10 | <DL | 3.54 | 2.82 | 0.803 | 7.71 | 13.2 | 0.022 | 3.58 | 0.697 |
| CaO | 6.65 | 8.79 | 11.3 | 8.80 | 10.0 | 0.207 | 0.009 | 7.37 | 14.0 | 12.0 | 22.3 | 0.454 | 6.55 | 10.8 |
| Na ₂ O | 0.013 | 0.012 | 8.00 | 3.50 | 3.57 | 11.7 | 0.677 | <DL | 0.026 | 7.86 | 1.58 | 11.4 | 0.039 | 0.044 |
| K ₂ O | 0.029 | 0.016 | <DL | 0.172 | 0.743 | 0.061 | 9.725 | 0.040 | 0.043 | 0.014 | <DL | <DL | <DL | <DL |
| Cr ₂ O ₃ | 0.002 | 0.032 | <DL | 0.012 | <DL | 0.014 | 0.023 | <DL | 0.115 | 0.061 | 0.033 | <DL | 0.0000 | 0.030 |
| Sum | 100.28 | 99.82 | 98.86 | 97.42 | 96.35 | 99.27 | 94.57 | 100.77 | 101.18 | 99.10 | 98.32 | 99.47 | 100.04 | 100.12 |
| Si | 5.96 | 5.97 | 2.01 | 7.53 | 6.31 | 2.97 | 6.82 | 6.07 | 6.09 | 2.01 | 2.00 | 2.96 | 6.01 | 6.05 |
| Ti | 0.009 | 0.018 | 0.001 | 0.014 | 0.004 | 0.00 | 0.018 | 0.008 | 0.022 | 0.001 | 0.003 | 0.000 | 0.006 | 0.012 |
| Al | 4.04 | 4.05 | 0.449 | 1.16 | 3.33 | 1.03 | 4.36 | 4.07 | 4.01 | 0.497 | 0.081 | 1.04 | 4.15 | 4.12 |
| Fe | 3.90 | 3.74 | 0.187 | 0.919 | 1.95 | 0.007 | 0.182 | 3.83 | 2.58 | 0.099 | 0.183 | 0.009 | 3.78 | 2.55 |
| Mn | 0.054 | 0.185 | 0.001 | 0.011 | 0.024 | 0.000 | 0.001 | 0.021 | 0.651 | 0.000 | 0.005 | 0.000 | 0.081 | 1.15 |
| Mg | 0.912 | 0.524 | 0.395 | 3.41 | 2.12 | 0.000 | 0.703 | 0.655 | 0.185 | 0.409 | 0.735 | 0.001 | 0.837 | 0.164 |
| Ca | 1.12 | 1.50 | 0.438 | 1.32 | 1.67 | 0.010 | 0.001 | 1.23 | 2.32 | 0.456 | 0.894 | 0.021 | 1.10 | 1.83 |
| Na | 0.004 | 0.004 | 0.562 | 0.951 | 1.08 | 0.998 | 0.175 | 0.000 | 0.008 | 0.542 | 0.115 | 0.976 | 0.012 | 0.014 |
| K | 0.006 | 0.003 | 0.00 | 0.031 | 0.148 | 0.003 | 1.65 | 0.080 | 0.008 | 0.001 | 0.000 | 0.000 | 0.000 | 0.000 |
| Cr | 0.000 | 0.004 | 0.00 | 0.001 | 0.000 | 0.000 | 0.000 | 0.000 | 0.014 | 0.002 | 0.001 | 0.000 | 0.000 | 0.004 |
| Sum | 16.01 | 15.99 | 4.04 | 15.36 | 16.64 | 5.02 | 13.90 | 15.89 | 15.87 | 4.01 | 4.01 | 5.01 | 15.94 | 15.89 |
| O | 24.00 | 24.00 | 6.00 | 23.00 | 23.00 | 8.00 | 22.00 | 24.00 | 24.00 | 6.00 | 6.00 | 8.00 | 24.00 | 24.00 |

Mg-Ca-Na-O system). There are currently no widely accepted solution models available for clinopyroxene and especially for amphibole. For both minerals, we have used an arbitrary ideal solution model. Further limitations arise from the fact that individual domains of the sample obviously equilibrated at different metamorphic stages, calling into question the use of bulk rock XRF major element data as a viable input composition. Nevertheless, the equilibrium phase diagram allows some conclusions about the P-T evolution. For the given bulk composition, the observed peak-pressure assemblage (Grt + Cpx1 + Qtz + Pg + Am) is predicted to be stable over a fairly large P-T range (500–700 °C and 12–20 kbar). Assuming that the pressure range inferred from barometry is correct, peak conditions should be around 550–600 °C and 17–19 kbar. The stability field of the peak-pressure assemblage is limited towards higher temperatures through the breakdown of paragonite which should decompose to form kyanite and clinopyroxene1 at higher pressures (assemblage 1 in Fig. 7) and plagioclase and amphibole at lower pressures (assemblage 3). The locations of the paragonite breakdown reactions in P-T space are relatively insensitive to the bulk composition and are in any case associated with dehydration. Thus we consider the presence of paragonite to be a robust constraint on P and T conditions. Hence, the equilibrium phase diagram indicates that pressures did not exceed 20 kbar and that decompression was associated with cooling, a conclusion that is also supported by the compositions of retrograde amphiboles and feldspar. The equilibrium phase diagram fur-

ther predicts the appearance of clinozoisite at conditions below 500 °C and 12 kbar. The peak P-T conditions proposed here agree well with independent P-T calculations on sample PIS1 (500–590 °C and 13–14.5 kbar minimum P) by Liati & Froitzheim (2006).

Some studies have inferred a reheating of samples from the southern flank of the Monte Rosa massif based on late generations of hornblende and plagioclase (e.g., Alta Luce, Borghi et al. 1996). In our samples, we observe the hornblende rims but could not identify Ca-bearing plagioclase. Our calculations predict decreasing glaucophane components in amphibole towards lower pressures even during cooling along the proposed P-T path. Given the limited coverage of this study, we do not exclude the possibility of a reheating event at low pressures. However, the persistence of large paragonite crystals, which were apparently part of the peak metamorphic assemblage, should constrain the temperatures to less than 500 °C at pressures below 10 kbar. Along the P-T path, garnet is most abundant at peak-pressure conditions. Because the chemical zonation of garnet is of a typical prograde nature, we propose that garnet growth in our samples occurred as pressures and temperatures increased during subduction to peak pressure conditions.

3. Analytical methods

Samples were crushed in a steel mortar and divided into two splits. One split was powdered in an agate mill and used for

major- and trace element analyses. The second split was used for mineral separation after the clay-size fraction was removed. Following separation of a garnet-rich fraction by a Franz LB-1 magnetic separator, visibly inclusion free garnet separates were hand picked mostly from the 128–180 μm size range. To avoid biasing the bulk garnet samples toward cores or rims, magnetic separator settings were chosen such that only a few impure garnet grains remained in the ‘garnet-poor’ fraction. However, because inclusion-free garnet fragments were preferred during handpicking, a bias towards the inclusion-poor garnet rims relative to the inclusion-rich garnet cores is likely. Sample PIS1 had already been crushed at ETH-Zürich and was used for zircon separation (Liati & Froitzheim 2006). From this sample, only the 63–128 μm size fraction was available for garnet picking. Garnet separates (100–150 mg) were cleaned in an ultrasonic bath with deionised water and dried. Whole-rock analyses were performed on representative sample powders.

All samples were spiked with mixed ^{176}Lu - ^{180}Hf and ^{149}Sm - ^{150}Nd tracers before digestion. Two different digestion procedures were applied. (1) The rutiles and one set of whole rock powders were digested in steel-jacketed PARR bombs with HF-HNO₃-HClO₄ for 24 hours at 180 °C. (2) To selectively dissolve the garnet fractions without digesting microscopic grains of Hf-bearing phases such as zircon, a tabletop procedure was applied, whereby samples are digested with HF-HNO₃-HClO₄ in closed Teflon vials on 120 °C hotplates as described in Lagos et al. (2007). Both digestion methods continue with samples being dried down on a hotplate, evaporating virtually all of the HClO₄, and re-dissolving in 6 M HCl. In most cases, the digestion procedure had to be repeated at least once to achieve a visibly clear sample solution. At this point, the sample was assumed to be fully equilibrated with spike. To screen for the presence of inherited zircon, which would affect the whole-rock Hf compositions, an additional set of whole rock samples was run through the tabletop digestion procedure. Sufficient amounts of significantly older inherited zircon would cause the bombed whole rock fraction to lie below – rather than on – a table-top digested whole rock – garnet isochron. All sample solutions were dried down, re-dissolved in 2.5 M HCl and centrifuged to remove any newly-formed precipitates or undigested minerals prior to loading onto cation exchange columns. A single-column separation procedure using Eichron Ln-Spec resin was used to separate Lu and Hf from the rock matrix (Münker et al. 2001). Apart from the Lu and Hf cuts, a matrix cut that included the LREE and MREE was collected. Two further column separation steps were carried out to purify Sm and Nd. The LREE and MREE were first separated from the matrix elements by using cation exchange resin (AG 50 W \times 12, 200–400 mesh) and 2.5 M HCl. The resulting REE fraction was collected in 6 M HCl. Samarium and Nd were then purified on a third column using HDEHP-coated Teflon beads after Richard et al. (1976).

Lutetium and Hf measurements were carried out in static mode using the Micromass Isoprobe MC-ICPMS at Universität Münster. Mass bias for Hf was corrected by using $^{179}\text{Hf}/^{177}\text{Hf}$ of 0.7325 (Patchett & Tatsumoto 1980) and the exponential law.

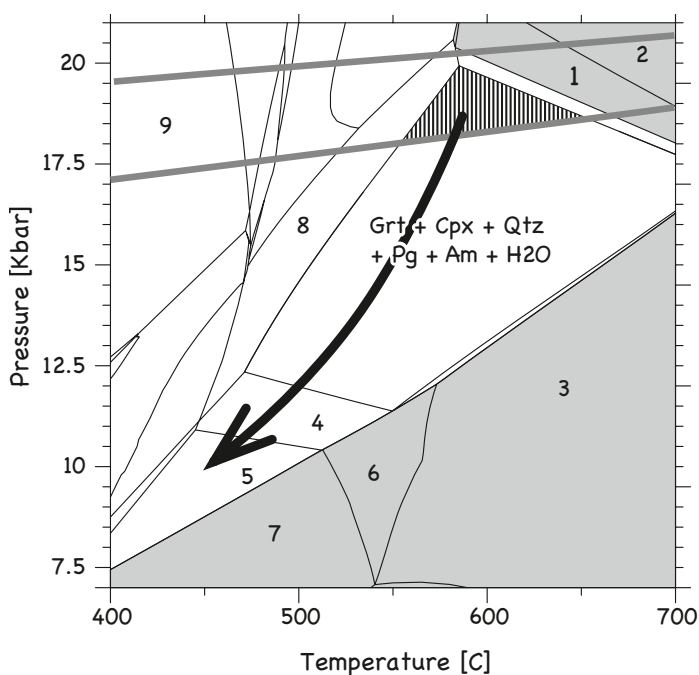


Fig. 7. Equilibrium phase diagram (De Capitani 1994) calculated for the bulk composition of sample MR56. Chemical system is Si-Al-Fe-Mg-Ca-Na-O. Light grey lines indicate range of Grt-Cpx-Png barometry in the same sample. Dark arrow indicates inferred P-T path. Grey shaded area indicates paragonite-free assemblages posing a robust constraint on the P-T path of the sample. Black and white shaded area indicates constraints on peak P-T conditions. Selected assemblages: (1) Grt + Cpx1 + Am + Qtz + Ky + H₂O, (2) Grt + Cpx + Qtz + Ky + H₂O, (3) Grt + Fsp + Cpx + Am + Qtz + H₂O, (4) Grt + Cpx + Qtz + Pl + Am + Czo + H₂O, (5) Cpx + Qtz + Pl + Am + Czo + H₂O, (6) Grt + Fsp + Cpx + Czo + Am + Qtz + H₂O, (7) Fsp + Cpx + Am + Qtz + H₂O, (8) Grt + Cpx + Qtz + Pl + Am + Lws + H₂O, (9) Cpx + Chl + Lws + Qtz + H₂O. Mineral abbreviations are after Kretz (1983); except: Am = amphibole.

Measured $^{176}\text{Hf}/^{177}\text{Hf}$ values are reported relative to $^{176}\text{Hf}/^{177}\text{Hf} = 0.282160$ for the Münster Ames Hf standard, which is isotopically identical to the JMC-475 standard. For the purpose of plotting isochrons, the external reproducibility of analyses was estimated using the empirical relationship 2σ (external 2 s.d.) = $\sim 2 \times 2\sigma_m$ (internal 2 s.e. run statistic) for replicate measurements of different concentrations of Hf standard solutions (see Bizzarro 2003). For interference corrections on ^{176}Hf and ^{180}Hf , the ^{173}Yb , ^{175}Lu , ^{181}Ta , and ^{182}W signals were monitored. For Lu measurements, mass bias correction and correction of the ^{176}Yb interference was achieved by monitoring the naturally occurring Yb in the Lu cuts and using the trend defined by $\ln(^{176}\text{Yb}/^{171}\text{Yb})$ vs. $\ln(^{173}\text{Yb}/^{171}\text{Yb})$ of Yb standard analyses that were interspersed with samples during the run sessions (e.g., Blichert-Toft et al. 2002; Albarède et al. 2004; Vervoort et al. 2004). This procedure typically results in an external reproducibility of $\sim 0.2\%$ (2σ) for the $^{176}\text{Lu}/^{177}\text{Hf}$ values of ideally spiked sample solutions. Blanks for Lu and Hf were <10 and <50 pg respectively.

Neodymium isotope ratios of whole rock samples were determined by MC-TIMS (Finnigan Triton) in Münster. The iso-

Table 2. XRF and LA-ICP-MS analyses for Balma eclogite samples PIS1, MR1, and MR56.

| | MR1 | MR56 | PIS1 |
|--|-------|-------|-------|
| <i>Major elements in weight percent oxides</i> | | | |
| SiO ₂ | 48.5 | 49.0 | 46.5 |
| TiO ₂ | 1.42 | 2.04 | 1.63 |
| Al ₂ O ₃ | 16.2 | 15.9 | 16.0 |
| Fe ₂ O ₃ | 9.62 | 10.8 | 15.0 |
| MnO | 0.18 | 0.18 | 0.28 |
| MgO | 7.84 | 6.56 | 6.62 |
| CaO | 10.6 | 10.6 | 10.9 |
| Na ₂ O | 3.46 | 3.08 | 2.47 |
| K ₂ O | 0.030 | 0.16 | 0.030 |
| P ₂ O ₅ | 0.302 | 0.186 | 0.067 |
| SO ₃ | 0.031 | 0.021 | 0.093 |
| <i>Trace elements (XRF) in ppm</i> | | | |
| Sc | 40 | 37 | 53 |
| V | 250 | 311 | 264 |
| Cr | 262 | 205 | 205 |
| Co | 40 | 39 | 47 |
| Ni | 133 | 96 | 83 |
| Cu | 39 | 49 | 18 |
| Zn | 141 | 83 | 83 |
| Ga | 12 | 22 | 19 |
| L.O.I. | 0.82 | 0.67 | 0.03 |
| Total (in%) | 99.09 | 99.28 | 99.82 |
| <i>Trace elements (LA-ICP-MS) in ppm</i> | | | |
| Cs | 0.044 | 0.11 | 0.67 |
| Rb | 0.33 | 2.4 | 0.22 |
| Ba | 10 | 6.6 | 7.3 |
| Th | 0.20 | 0.24 | 0.19 |
| U | 0.11 | 0.15 | 0.17 |
| Nb | 2.4 | 3.6 | 3.4 |
| Ta | 0.16 | 0.21 | 0.20 |
| La | 7.5 | 8.1 | 6.2 |
| Ce | 13 | 18 | 12 |
| Nd | 13 | 19 | 12 |
| Zr | 112 | 168 | 171 |
| Hf | 2.8 | 4.0 | 4.0 |
| Pr | 2.2 | 3.3 | 2.0 |
| Sm | 4.2 | 6.0 | 3.7 |
| Eu | 1.5 | 2.0 | 1.3 |
| Gd | 5.0 | 7.5 | 5.3 |
| Tb | 0.77 | 1.1 | 1.3 |
| Ho | 1.2 | 1.8 | 2.6 |
| Y | 29 | 45 | 67 |
| Er | 3.4 | 5.0 | 7.6 |
| Tm | 0.45 | 0.71 | 1.1 |
| Yb | 3.1 | 5.1 | 7.4 |
| Lu | 0.41 | 0.7 | 1.1 |

baric interference on ¹⁴⁴Nd was corrected by monitoring ¹⁴⁷Sm and using the natural ¹⁴⁷Sm/¹⁴⁴Sm. Mass fractionation was corrected using a ¹⁴⁶Nd/¹⁴⁴Nd of 0.7219 and the exponential law. The typical reproducibility of ¹⁴³Nd/¹⁴⁴Nd values is ± 50 ppm. A value of 0.511847 was obtained for the LaJolla Nd standard during the course of this study.

X-ray fluorescence analyses of major and trace elements in whole rock samples were carried out at the Steinmann-Institut Bonn, and electron microprobe work was conducted at the Institut für Geologie und Mineralogie in Cologne. Further trace element abundances in whole rock samples were analysed by melting the samples with lithium tetraborate. The resulting fused disks were analysed directly using the Thermo Finnigan Element2 LA-SF-ICP-MS at the Max-Planck-Institut für Chemie in Mainz. Analyses of Nist 612 SRM reference glass measured together with the samples indicate, that the 95% confidence level of trace element concentration is usually better than 5–10% of the sample concentration (Jochum et al. 2007).

4. Results

4.1 Major and trace elements

Major and trace element data for the eclogite samples are given in Table 2. All samples have similar basaltic compositions with 46.4–49.0 wt% SiO₂, Al₂O₃ of 15.9–16.2 wt% and 6.56–7.84 wt% MgO. Titanium contents are high (1.42–2.04 wt%) and Zr contents are moderately high for mafic rocks (113–173 ppm). Chondrite-normalized REE patterns reveal that sample PIS1 is clearly depleted in LREE, whereas samples MR1 and MR56 have rather flat patterns with a slight enrichment in LREE (Fig. 8a). Extended trace element patterns normalized to primitive mantle are similar to those of typical N-MORB (Hofmann 1988). There appears to be evidence for U and LREE mobility, as indicated by a U-enrichment in all samples and a positive Zr-Hf anomaly in sample PIS1 (Fig 8b). Element concentrations are given in Table 2.

All measured garnets are typical almandine-rich, eclogitic garnets. Element profiles across representative garnets show characteristic zoning patterns of Fe, Mg, Mn, and Ca. Bell-shaped manganese profiles are generally interpreted to indicate original prograde growth zoning in garnet (Spear 1991; Kohn 2003). In addition to this observation, molar Fe²⁺/(Fe²⁺+Mg²⁺) decreases from core to rim in all samples. Some garnets show slight enrichment of spessartine component at the outer garnet rim which could be interpreted either as the result of garnet dissolving on a retrograde PT path or by breakdown of a Mn-rich phase during a late stage of garnet growth.

4.2 Lu-Hf geochronology

Figure 9 illustrates the ¹⁷⁶Hf/¹⁷⁷Hf and Lu-Hf results for the three analysed samples in Lu-Hf isochron space. Isochron regressions were calculated using ISOPLOT v. 2.49 (Ludwig 2001), using the 2σ uncertainties in ¹⁷⁶Lu/¹⁷⁷Hf (Table 3), and 2σ uncertainties in ¹⁷⁶Hf/¹⁷⁷Hf estimated from the 2σ_m internal run statistics as previously described. Calculated ages are based on the decay constant of λ¹⁷⁶Lu = 1.865 × 10⁻¹¹ yr⁻¹ (Scherer et al. 2001; corroborated by Söderlund et al. 2004).

Hafnium contents in the whole rocks range from 0.4 to 1.3 ppm. The garnets have Hf contents of 30 to 93 ppb and

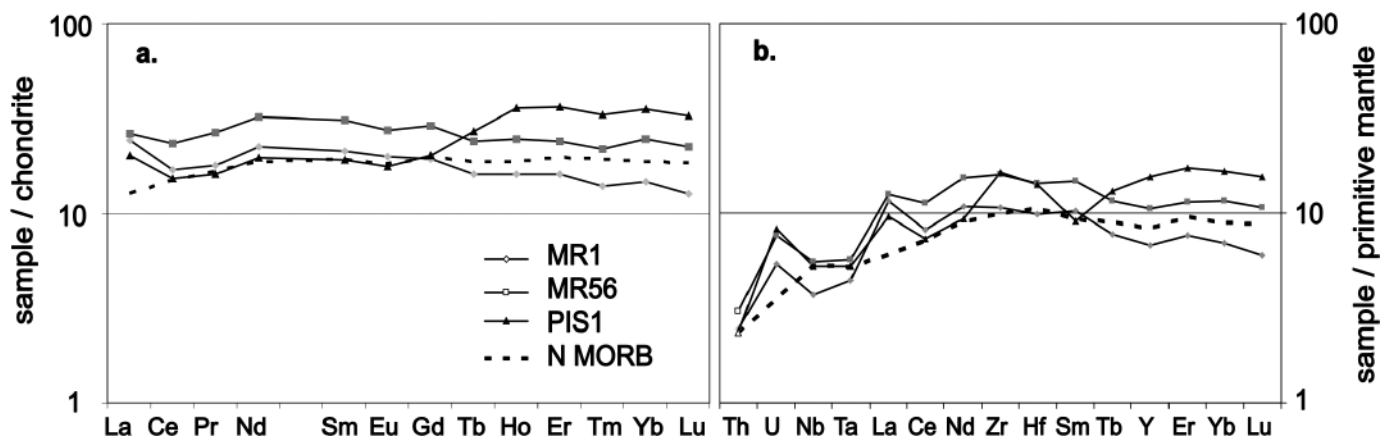


Fig. 8. (a) Chondrite-normalized REE diagram (values from Boynton 1984), showing compositions of the Balma eclogites in comparison to those of N-MORB (values are taken from Hofmann 1988). (b) Incompatible trace element diagram, normalized to primitive mantle (McDounough & Sun 1995).

Table 3. Lu and Hf concentrations and Hf-Nd isotope data for Balma eclogite samples PIS1, MR1 and MR56. ‘Whole rock 1’ fractions were digested via the selective tabletop digestion procedure; ‘whole rock 2’ fractions were digested in bombs. Uncertainties on the last decimal places (in parentheses) are estimated 2σ external reproducibility for $^{176}\text{Lu}/^{177}\text{Hf}$ and $^{147}\text{Sm}/^{144}\text{Nd}$, and $2\sigma/\sqrt{n}$ internal run statistics for $^{176}\text{Hf}/^{177}\text{Hf}$ and $^{143}\text{Nd}/^{144}\text{Nd}$. For the purpose of plotting Lu-Hf isochrons, the 2σ uncertainties on $^{176}\text{Hf}/^{177}\text{Hf}$ are estimated using the method of Bizzarro et al. (2003). See text for details. The 93 Ma zircon protolith age (Liati & Froitzheim 2006) is used to calculate $\epsilon\text{Hf}(t)$ and $\epsilon\text{Nd}(t)$.

| fraction | ppm Lu | ppm Hf | $^{176}\text{Lu}/^{177}\text{Hf}$ | $^{176}\text{Hf}/^{177}\text{Hf}$ | $\epsilon\text{Hf}(0)$ | $\epsilon\text{Hf}(t)$ |
|---------------------|--------|--------|-----------------------------------|-----------------------------------|------------------------|------------------------|
| <i>sample: PIS1</i> | | | | | | |
| rutile 1 | 0.0212 | 2.02 | 0.001491 (8) | 0.283242 (20) | | |
| rutile 2 | 0.0162 | 0.326 | 0.00706 (2) | 0.282980 (32) | | |
| whole-rock 1 | 0.597 | 0.441 | 0.1922 (3) | 0.283314 (25) | 19.2 | 10.7 (9) |
| whole-rock 2 | 0.977 | 1.19 | 0.1170 (2) | 0.283230 (8) | 16.2 | 11.8 (5) |
| garnet 1 | 1.88 | 0.113 | 2.361 (4) | 0.284977 (25) | | |
| garnet 2 | 2.04 | 0.101 | 2.858 (5) | 0.285395 (21) | | |
| garnet 3 | 1.68 | 0.0927 | 2.576 (5) | 0.285190 (22) | | |
| <i>sample: MR1</i> | | | | | | |
| rutile 1 | 0.0158 | 1.11 | 0.00201 (1) | 0.283258 (23) | | |
| rutile 2 | 0.0108 | 0.260 | 0.00587 (2) | 0.283448 (57) | | |
| whole-rock 1 | 0.492 | 0.400 | 0.1747 (3) | 0.283325 (15) | 19.5 | 12.0 (5) |
| whole-rock 2 | 0.410 | 0.872 | 0.06671 (13) | 0.283190 (8) | 14.8 | 13.0 (5) |
| garnet 1 | 1.26 | 0.0433 | 4.128 (8) | 0.286436 (56) | | |
| garnet 2 | 1.30 | 0.0321 | 5.752 (10) | 0.287797 (22) | | |
| garnet 3 | 1.28 | 0.0297 | 6.126 (11) | 0.288053 (47) | | |
| <i>sample: MR56</i> | | | | | | |
| rutile | 0.0162 | 0.208 | 0.01104 (3) | 0.283015 (37) | | |
| whole-rock 1 | 0.620 | 0.433 | 0.2031 (4) | 0.283294 (16) | 18.5 | 9.5 (11) |
| whole-rock 2 | 0.659 | 1.33 | 0.07025 (15) | 0.283179 (8) | 14.4 | 12.5 (6) |
| garnet 1 | 1.85 | 0.0534 | 4.922 (9) | 0.287246 (36) | | |
| garnet 2 | 1.78 | 0.0465 | 5.437 (10) | 0.287747 (21) | | |
| garnet 3 | 1.85 | 0.0358 | 7.344 (14) | 0.289348 (36) | | |
| fraction | ppm Sm | ppm Nd | $^{143}\text{Nd}/^{144}\text{Nd}$ | $^{147}\text{Sm}/^{144}\text{Nd}$ | $\epsilon\text{Nd}(0)$ | $\epsilon\text{Nd}(t)$ |
| <i>sample: PIS1</i> | | | | | | |
| whole-rock 1 | 4.548 | 14.27 | 0.513001 (158) | 0.1927 (4) | 7.1 | 7.1 (31) |
| whole-rock 2 | 3.448 | 10.489 | 0.513088 (10) | 0.1990 (4) | 8.8 | 8.8 (2) |
| <i>sample: MR1</i> | | | | | | |
| whole-rock 1 | 3.787 | 11.47 | 0.513095 (6) | 0.1996 (4) | 8.9 | 8.9 (2) |
| whole-rock 2 | 3.863 | 11.67 | 0.513093 (9) | 0.2001 (4) | 8.9 | 8.9 (2) |
| <i>sample: MR56</i> | | | | | | |
| whole-rock 1 | 4.914 | 14.76 | 0.513094 (12) | 0.2014 (4) | 8.9 | 8.9 (2) |
| whole-rock 2 | 5.549 | 16.62 | 0.513095 (10) | 0.2019 (4) | 8.9 | 8.9 (2) |

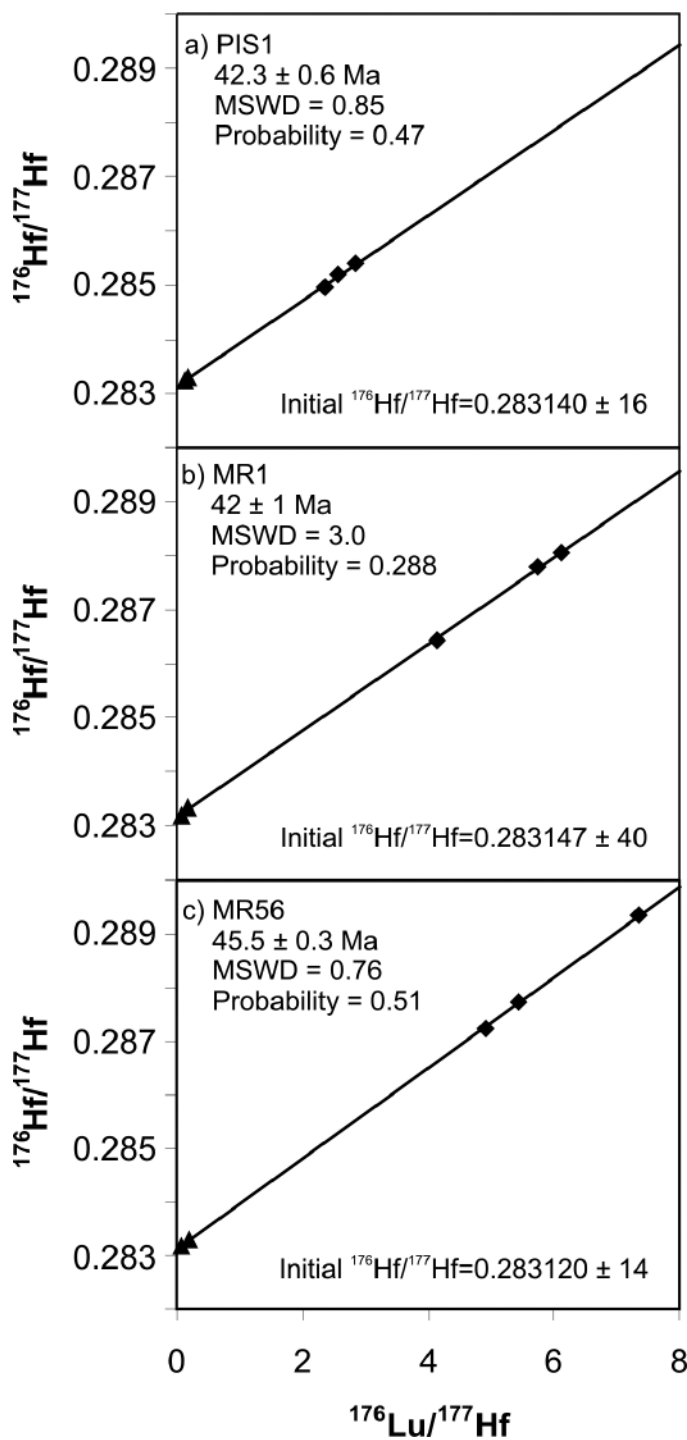


Fig. 9. Lu-Hf garnet (diamonds) whole rock (triangle) isochron plots for samples a) PIS1, b) MR1 and c) MR56. 2σ uncertainties used in regressions are always smaller than symbol sizes. Calculated initial values and ages are based on $\lambda^{176}\text{Lu} = 1.865 \times 10^{-11} \text{ yr}^{-1}$ (Scherer et al. 2001).

$^{176}\text{Lu}/^{177}\text{Hf}$ ranging from 2.36 to 7.34. For each sample, both whole rock splits and all three garnet separates measured define isochrons, suggesting that sample-spike equilibration was achieved during the selective digestion procedure used for

garnets and whole rock split. The two rutile separates analysed for each sample however, do not plot on these isochrons, possibly indicating the lack of full isotopic equilibrium between the rutile fraction and their host rocks at the time of their crystallization or that the rutile crystallized at a different time than garnet. The Lu-Hf garnet-whole-rock ages that have been obtained for eclogites from the Balma unit (Fig. 9) are 42.3 ± 0.6 , 42 ± 1 and 45.5 ± 0.3 Ma. These ages are younger than all Lu-Hf ages established so far for South Penninic Units (Fig. 10).

5. Discussion

5.1 Significance of Lu-Hf Ages

If Lu-Hf garnet geochronology is to be applied to determine prograde growth ages, the following criteria have to be met: (1) garnet rims must have been in isotopic equilibrium with the whole rock matrix during garnet growth, (2) the garnets must have remained closed systems for Lu and Hf since their formation, and (3) the garnet separates analysed must not contain any significantly older inherited components, such as zircon (e.g., Scherer et al. 2000). The Lu-Hf closure temperature (T_c) after Dodson (1973) depends on multiple factors such as peak temperature, cooling rate, mineral composition, and grain size and shape. The latter, along with presence of inclusions and their distribution, affect the effective diffusion radii. Only one direct estimate for T_c of Lu-Hf isotopic system in garnets has been proposed: about 720–755 °C for rapid cooling rates (Skora et al. 2006b). Most other estimates were made relative to the T_c of the Sm-Nd isotope system in garnet (e.g., Scherer et al. 2000; Lapen et al. 2003). These authors predict that T_c for the Lu-Hf system is higher than for the Sm-Nd isotope system in the same garnet. Numerous T_c estimates for Sm-Nd in garnet have been published (Jagoutz 1988; Cohen et al. 1988; Mezger et al. 1992; Burton et al. 1995; Hensen & Zou 1995; Becker 1997; Scherer et al. 2000; Van Orman et al. 2002; Thoeni 2002; Tirone et al. 2004), ranging between 490 °C for 0.2 mm size garnets and low cooling rates to 1050 °C for 3 mm size garnets and high cooling rates. The garnet porphyroblasts studied here have experienced peak temperatures of only 550–600 °C and are therefore unlikely to have undergone Lu or Hf exchange with their surroundings after their growth. This, together with the preserved prograde growth zoning in Mn^{2+} , which, according to Van Orman et al. (2002), would diffuse faster than 3^+ ions (e.g., Lu) and probably also 4^+ ions (e.g., Hf), suggests that the Lu-Hf ages reflect garnet growth rather than cooling ages.

The effects of trace mineral inclusions on Lu-Hf garnet geochronology were investigated by Scherer et al. (2000). Hafnium-rich inclusions, such as zircon and rutile, can lower the Lu/Hf and $^{176}\text{Hf}/^{177}\text{Hf}$ of a bulk garnet separate relative to those of pure garnet. Zircon is the most problematic of these minerals for Lu-Hf garnet dating because it may contain a significantly older inherited component that did not isotopically equilibrate with the whole rock at the time of garnet nucleation. In such a case, measured $^{176}\text{Lu}/^{177}\text{Hf}$ and $^{176}\text{Hf}/^{177}\text{Hf}$ values would lie on

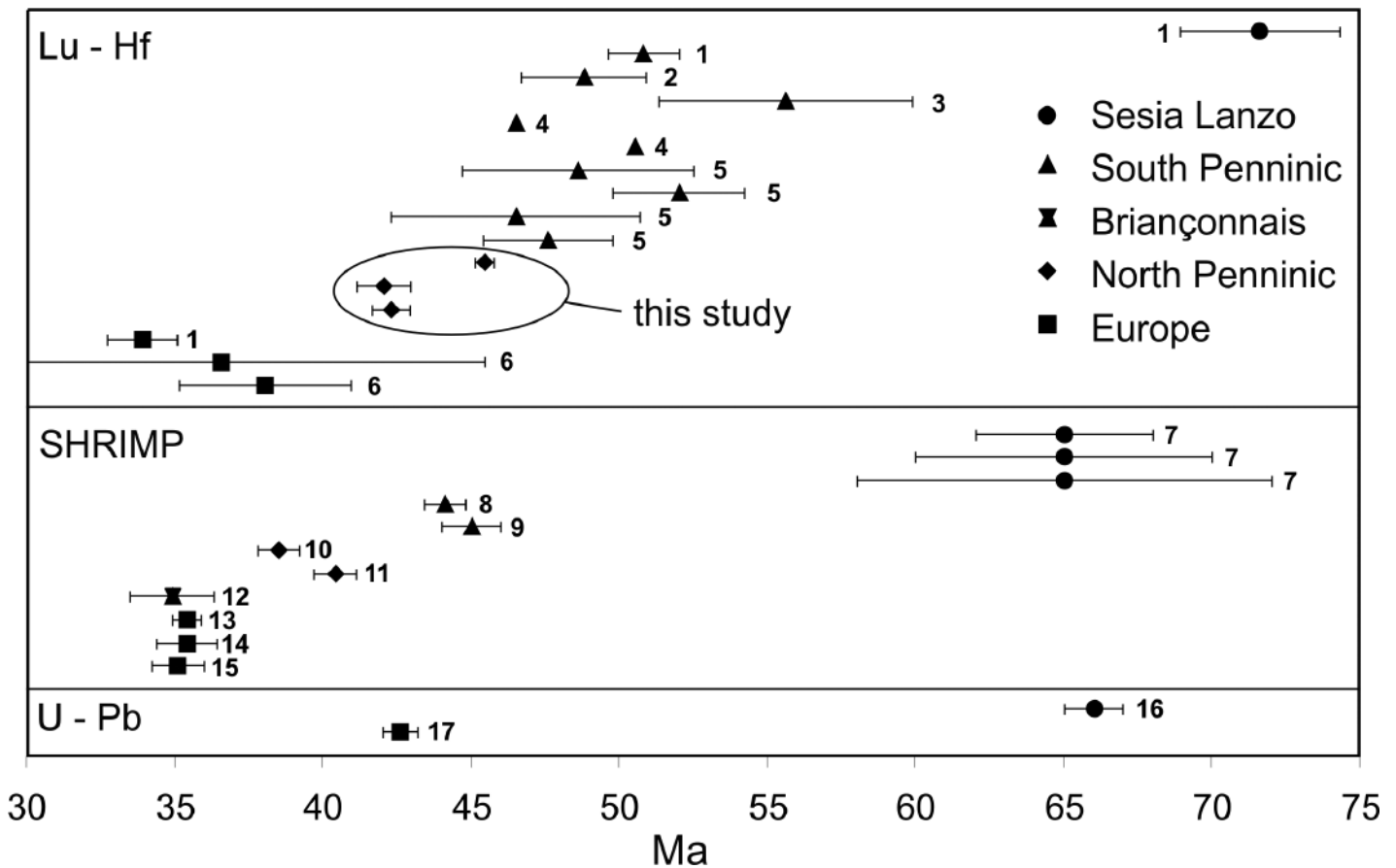


Fig. 10. Ages of HP and UHP metamorphism established in the western and central Alps over the last 10 years by Lu-Hf garnet, U-Pb SHRIMP-zircon, and U-Pb-rutile dating (1) Duchêne et al. (1997) recalculated with the decay constant of Scherer et al. (2001), (2) Lapen et al. (2003), (3) Mahlen et al. (2003), (4) Mahlen et al. (2005), (5) Mahlen et al. (2006), (6) Brouwer et al. (2005), (7) Rubatto et al. (1999), (8) Rubatto et al. (1998), (9) Rubatto & Hermann (2003), (10) Liati et al. (2005), (11) Liati & Froitzheim (2006), (12) Rubatto & Gebauer (1999), (13) Gebauer et al. (1996), (14) Gebauer et al. (1997), (15) Rubatto & Hermann (2001), (16) Inger et al. (1996), (17) Lapen et al. (2007). The Lu-Hf ages of 36.6 ± 8.9 and 38.1 ± 2.9 Ma (Brouwer et al. 2005) come from Alpe Arami and Gorduno, respectively. Further Lu-Hf garnet ages by Brouwer et al. (2005) are not discussed, as their paleogeographic origin is difficult to interpret and/or they contain older components.

mixing lines between pure garnet and zircon and whole rock (minus its zircon) and zircon, thus potentially producing an age bias. Zircon inclusions are commonly submicroscopic, and even the most carefully handpicked garnet separates may contain them. Rutile is part of the high pressure assemblage but may also carry an inherited Hf isotope signature, perhaps in the form of zircon inclusions. This might be the case for the Balma samples as some of the rutile separates plot below their respective isochrons. Other rutile separates plot above the garnet-whole rock isochrons, suggesting that their Hf may be derived from the breakdown of more radiogenic minerals. In the case of initial isotopic equilibrium among all mineral phases, the resulting lower Lu/Hf of zircon- or rutile-bearing garnet separates merely affect the precision of the age calculated and not its accuracy. To minimize inclusion effects, (1) the separates were carefully handpicked and (2) a selective tabletop digestion procedure was applied, as previously described. For all three cases, all garnet separates plot on isochrons with both

table-top- and bomb-digested whole rock fractions, suggesting that full sample-spike equilibrium was achieved and that any zircon present contains little if any significantly older inherited Hf component.

Despite the fact that all three samples originate from the same tectonic unit, the calculated Lu-Hf age of MR56 clearly differs from that of the other two samples. The cause of this age difference may include one or both of the following explanations: (1) If the garnet porphyroblasts grew over a long time interval (several million years), it is possible that different core-to-rim Lu distributions would bias Lu-Hf ages of different samples towards different parts of the growth intervals. Such Lu zoning can be produced by Rayleigh fractionation during garnet growth (Lapen et al. 2003) or by diffusion-limited garnet growth (Skora et al. 2006). Modelling by Skora et al. (2006) suggests that at low temperatures, diffusion-limited garnet growth might even lead to a situation where Lu concentrations in garnet rims are in fact higher than in garnet cores.

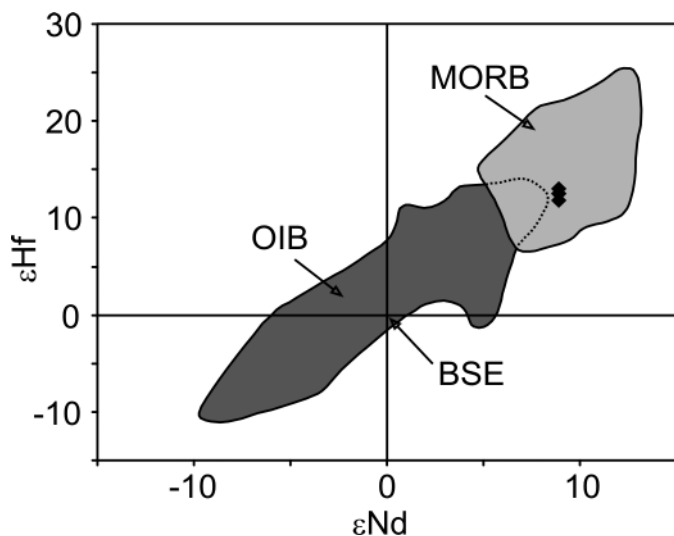


Fig. 11. Initial Hf-Nd isotope compositions (t at 93 Ma) of eclogites from the Balma Unit compared to compositions of MORB and OIB (Salters & White 1998; Chauvel & Blichert-Toft 2001 and references therein). Whole rock samples plotted here were all dissolved in PARR Bombs. 2σ errors are approximately symbol size. BSE values for Hf are taken from Blichert-Toft & Albarède (1997); values for Nd from (Jacobsen & Wasserburg 1980).

In the absence of trace element profiles through the garnets in this study, neither of these two explanations can be excluded. (2) As inclusion-free garnet fragments were preferred during hand picking, there might be a systematic bias towards inclusion-poor rim material. We therefore tentatively interpret the garnet ages to be weighted towards the later part of the garnet growth interval.

Even with the small age difference among the three eclogites, all of the Lu-Hf ages are consistently older than the U-Pb SHRIMP age of a metamorphic zircon rim in sample PIS1 (40.4 ± 0.7 Ma, Liati & Froitzheim 2006). The offset of two to five Myr between the two chronometers is not unusual and can be seen in almost all Alpine units (Fig. 10), except for the Dora-Maira Massif, where coesite-bearing quartzites, rather than eclogites, were used for zircon dating (Gebauer et al. 1997; Duchêne et al. 1997). In addition, the Lu-Hf age established by Duchêne et al. (1997) for Dora Maira was based on only a single two-point isochron. The consistent age differences between U-Pb zircon ages and Lu-Hf ages of garnet growth indicate that zircon growth most likely postdates garnet nucleation, which occurred during subduction-driven prograde metamorphism.

5.2 Characterisation of the protolith

An assessment of the tectonic setting (MORB vs. OIB origin) of the Balma metabasites (especially sample PIS1) can contribute to the paleogeographic assignment of the Balma unit.

Rare earth element patterns presented in Fig. 8a show a consistent depletion of LREE relative to HREE, suggesting a MORB origin. However, a depletion of LREE might also reflect fluid-rock interaction due to subduction-related dehydration

(e.g., John et al. 2004). Light REE and U are likely to be mobilized, whereas HREE, Nb, Ta, Zr, and Hf are often relatively immobile. This appears to be the case for sample PIS1, which is strongly depleted in LREE and shows a markedly positive Zr-Hf anomaly. In contrast, samples MR1 and MR56 do not show Zr-Hf anomalies and exhibit flat REE patterns. Hence, the combined trace element evidence from the three eclogite samples suggests an origin of the eclogites from MORB protoliths. Consistently high Zr/Nb ratios (46–50) also confirm a depleted mantle source.

Initial Hf and Nd isotope ratios obtained for the whole rocks clearly plot inside the field of MORB (Salters & White 1998; Chauvel & Blichert-Toft 2001 and references therein, Fig. 11). Even though trace element patterns show that Nd may have been mobile during subduction, the ϵ_{Nd} and ϵ_{Hf} values of all three samples broadly overlap, indicating that the Nd isotope composition was not significantly disturbed. Because zircon is not effectively dissolved by the table top digestion procedure, only Hf data from whole rocks digested in PARR-bombs were plotted in Fig. 11.

Collectively, the combined trace element and isotope evidence strongly suggest that the protolith for the studied eclogites was a MORB, thus precluding the possibility that the Cretaceous protolith age of sample PIS1 (Liati & Froitzheim 2006) reflects late ocean island magmatism.

5.3 Previous geochronological results from the Penninic nappes

Ophiolite protolith ages: Jurassic protolith ages of ca. 164 Ma (U-Pb SHRIMP on zircon) were determined for metagabbros of the Zermatt-Saas Zone by Rubatto et al. (1998). All protolith ages from South Penninic ophiolites in the Central and Western Alps range between ca. 142 and ca. 166 Ma (e.g., Kaczmarek et al. 2008; review of data in Liati et al. 2003). Jurassic SHRIMP ages of ca. 155, 158, and 156 Ma, were also determined for metagabbro, amphibolitized eclogite, and amphibolite of the Antrona Unit (Fig. 1, 2) by Liati et al. (2005). The Antrona ages were interpreted to indicate that this unit is a piece of South Penninic Ocean floor that was geometrically captured in the North Penninic Basin by sinistral movement (Fig. 2; Liati et al. 2005). As mentioned above, eclogite sample PIS1 from the Balma Unit yielded a Cretaceous protolith age of 93.4 ± 1.7 Ma (Cenomanian-Turonian; Liati & Froitzheim 2006). The age from the Balma Unit is identical to two ages (93.0 ± 2.0 and 93.9 ± 1.8 Ma, Liati et al. 2003) determined on amphibolites of the Chiavenna Ophiolite in the eastern Central Alps, for which an origin from the North Penninic Ocean is widely accepted (e.g., Schmid et al. 1996).

High-pressure metamorphism: Until ca. 1995; the high-pressure metamorphism in the Penninic Nappes was generally assumed to be Cretaceous in age, mostly based on K-Ar and ^{40}Ar - ^{39}Ar geochronology (compromised by excess argon). However, the application of U-Pb, Sm-Nd, and Lu-Hf geochronology has

shown that the high-pressure metamorphism is Tertiary in age, except for the Sesia Nappe, which already had experienced eclogite-facies metamorphism in the Latest Cretaceous. The ages decrease from the upper to the lower tectonic units, that is, from southeast to northwest in terms of paleogeography. More recent ^{40}Ar - ^{39}Ar work has confirmed the Tertiary ages (Dal Piaz et al. 2001; Agard et al. 2002; Bucher et al. 2003). Lutetium-Hf and U-Pb ages are compiled in Fig. 10 and discussed below with our tentative tectonic model (Fig. 12).

5.4 Tectonic implications

Our study provides additional support for a MORB origin of the protoliths. Together with the previously published ca. 93 Ma protolith age, this strengthens the evidence that oceanic spreading was still active in the Late Cretaceous. According to a plate tectonic model for the Alpine paleogeography (Stampfli & Borel 2004), spreading in the South Penninic Ocean took place in the Jurassic (Fig. 12a) and ceased by the Early Cretaceous (Barremian to Aptian), whereas the North Penninic Ocean opened in the Cretaceous (Fig. 12b). Geochronological data from South Penninic ophiolites and biochronological data from their cover units indicate that spreading began during the Bajocian and ended in the Kimmeridgian (Bill et al. 2001). This reflects the northward propagation of the Atlantic opening past Iberia. In the Jurassic, the northern tip of the North Atlantic ridge was at the latitude of Gibraltar, and Atlantic opening was transferred into the South Penninic (Piemont-Ligurian) Ocean through a strike-slip zone south of Iberia. During the Early Cretaceous, Atlantic opening propagated west of Iberia and was transferred to the North Penninic (Valais) Ocean through a transtensional zone between Iberia and Europe. Therefore, our geochemical results, together with the Late Cretaceous protolith age, support the interpretation of the Balma Unit as North Penninic.

Figure 12 shows a tentative reconstruction of the paleotectonic evolution assuming that the Balma Unit is indeed North Penninic. In this case, the South Penninic and North Penninic oceans must have been consumed by two separate subduction zones. If only one subduction zone had existed, the paleogeographic units should have arrived in this subduction zone one after the other, starting with the South Penninic units and ending with the European margin. The presently available Lu-Hf data (Fig. 10), however, suggest that subduction of the North Penninic Ocean started when subduction of the South Penninic Ocean was still going on or had just ended. This leaves no time for the subduction of the lithosphere which carried the Briançonnais units. Our tentative model presented in Fig. 12 therefore includes two partly contemporaneously active subduction zones: one consuming the South Penninic and the other subducting the North Penninic Ocean. The Lu-Hf ages presented here, as well as all other published U-Pb SHRIMP and Lu-Hf data for the western and central Alps, fit well into this model. As pointed out before and illustrated in Fig. 10, U-Pb SHRIMP ages seem to be offset relative to Lu-Hf garnet

ages by roughly 4 Myr. This is interpreted to indicate that metamorphic zircon crystallized after garnet had already nucleated along the prograde path. If our garnets are indeed biased by hand-picking towards inclusion free rims, this would place zircon growth in the latter part of – or even after – the garnet growth interval.

Eclogites from the Sesia Nappe yielded ages of 71.6 Ma using Lu-Hf (Duchêne et al. 1997 recalculated with the decay constant of Scherer et al. 2001) and of ca. 65 Ma using U-Pb on sphenes (Inger et al. 1996) and U-Pb SHRIMP on zircon (Rubatto et al. 1999) (Fig. 12c). In units from the South Penninic Ocean (Zermatt-Saas Zone, Monviso Unit) eclogite-facies metamorphism has been dated at 60 ± 12 and 62 ± 9 Ma (Sm-Nd garnet ages by Cliff et al. 1998) (Fig. 12d). However, most Lu-Hf ages cluster around 49 Ma (Duchêne et al. 1997 recalculated with the decay constant of Scherer et al. 2001; Lapen et al. 2003; Mahlen et al. 2003, 2005, 2006) (Fig. 12e), and U-Pb SHRIMP ages are again slightly younger (44.1 ± 0.7 and 45 ± 1 Rubatto et al. 1998; Rubatto & Hermann 2003) (Fig. 12f). Lutetium-Hf ages of 45.5 ± 0.3 , 42 ± 1 and 42.3 ± 0.6 Ma (this study) for North Penninic Ophiolites (Fig. 12f, g), suggest that subduction of the North Penninic Ocean started roughly at around 50 Ma (Fig. 12e). Once again, U-Pb SHRIMP ages (37.1 ± 1.9 , 38.5 ± 0.7 and 40.4 ± 0.7 Ma, Liati et al. 2003; 2005 and Liati & Froitzheim 2006) (Fig. 12h) are younger than the Lu-Hf ages, not only for the same unit but in this case even for the same sample: Sample PIS1 was analyzed by both methods and yields a U-Pb SHRIMP age of 40.4 ± 0.7 Ma (Liati & Froitzheim 2006) and a Lu-Hf age of 42.3 ± 0.6 Ma (this study). The first HP ages in the European margin, more precisely in the Monte Rosa Nappe, are 42.6 Ma (Lapen et al. 2007) using U-Pb in rutile (Fig. 12g). However, it must be stressed that the paleogeographic position of the Monte Rosa Nappe is controversial. A ca. 35 Ma U-Pb SHRIMP age has been published for the Gornergrat series (Rubatto & Gebauer 1999), which was attributed to the Monte Rosa Nappe by these authors, but according to our tectonic interpretation it rather belongs to the St. Bernard Nappe (Briançonnais). This age is therefore difficult to interpret. Lu-Hf garnet ages of 36.6 ± 8.9 and 38.1 ± 2.9 Ma (Brouwer et al. 2005) from the Adula Nappe (European margin) are in good agreement with 35.4 ± 0.5 Ma U-Pb SHRIMP ages from the same area determined by Gebauer et al. (1996) (Fig. 12i). Similar ages were determined for UHP metamorphism in the Dora-Maira Unit (which also belongs to the European margin according to our interpretation): 35.4 ± 1 and 35.1 ± 0.9 Ma using U-Pb SHRIMP (Gebauer et al. 1997; Rubatto & Hermann 2001) and 34.1 ± 1.2 Ma using Lu-Hf (Duchêne et al. 1997 recalculated with the decay constant of Scherer et al. 2001). This is the only occasion where a Lu-Hf age (two point isochron) is not significantly older than associated U-Pb SHRIMP ages, which could be due to the fact that coesite-bearing quartzites rather than eclogites were analyzed (Gebauer et al. 1997; Duchêne et al. 1997). Fig. 12j shows our tentative model for the Western Alps, taking into account the slab extraction model after Froitzheim et al. (2003). Such an event could have triggered ca. 33–30 Ma

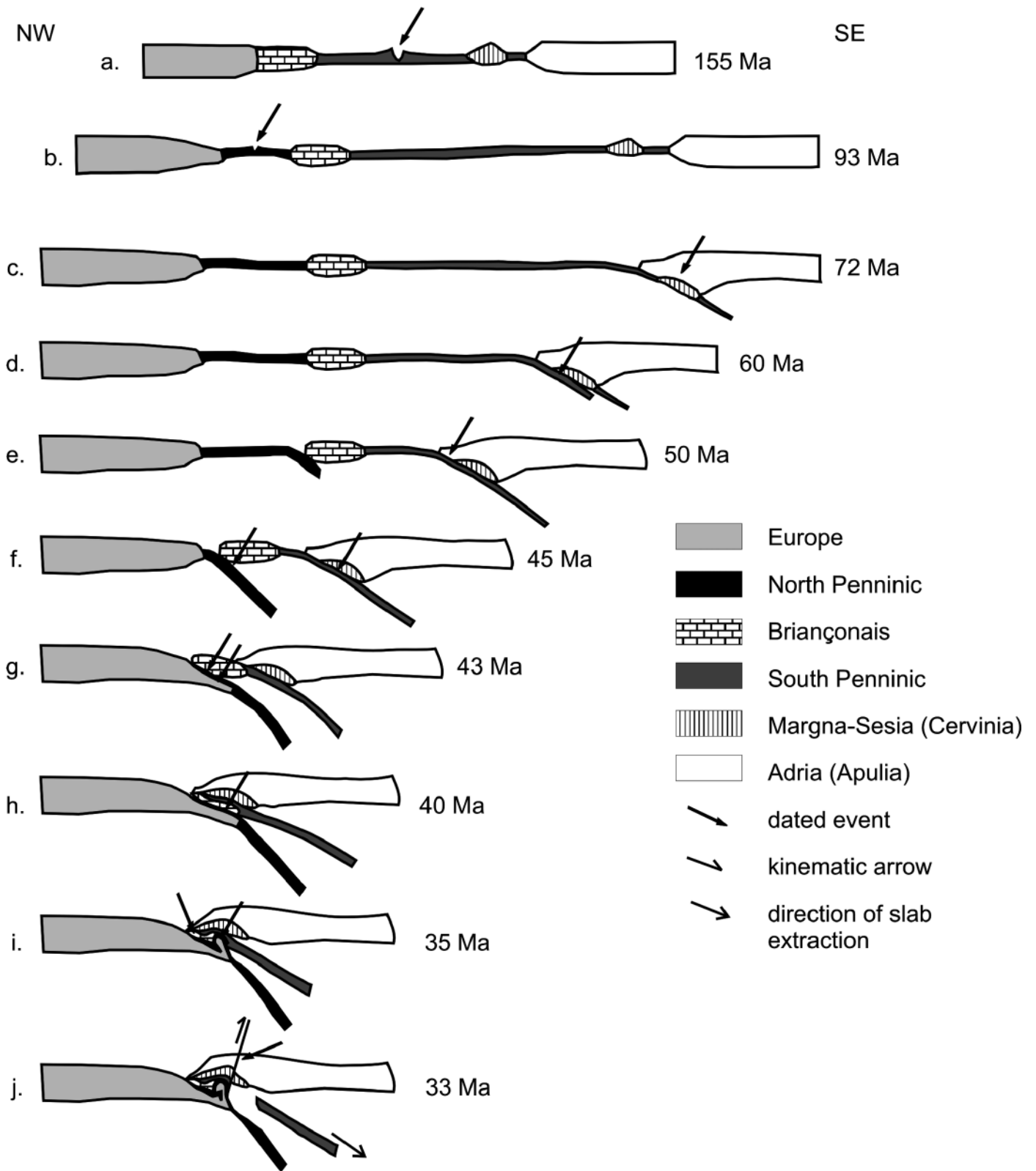


Fig. 12. Tentative model for the paleotectonic evolution of the western Alps, showing the spreading and the subduction of the South and North Penninic Oceans. All published Lu-Hf and U-Pb SHRIMP ages are consistent with this model as discussed in the text, and indicated by arrows. (j) is taking into account the slab extraction model after Froitzheim et al. (2003) (lower arrow). Such an event could have triggered ca. 33–30 Ma old magmatism along the Insubric lineament (kinematic arrow). Sketches have not been scaled for convergence rate or subduction depth.

old magmatism along the Insubric lineament (e.g. Oberli et al. 2004).

6. Conclusions

Our combined major- and trace element and Lu-Hf data for eclogites from the Balma Unit provide new constraints on the tectonic evolution of the western Alps. Previous models can now be modified as follows:

- 1) Trace elements and initial Hf-Nd isotope data strongly suggest that MORB-type ocean crust provides the protolith for the Balma eclogites. Consequently, the Cretaceous U-Pb SHRIMP age of synmagmatic zircon cores established from sample PIS1 (Liati & Froitzheim 2006) does not relate to late OIB magmatism in the South Penninic Ocean. Rather, the Balma unit was apparently derived from the North Penninic Ocean because that ocean was still actively spreading at the time.
- 2) Lutetium-Hf garnet ages obtained for three eclogites from the Balma unit range from 42 to 45.5 Ma and are systematically younger than those reported for South Penninic units (46.5–55.6 Myr).
- 3) In most cases Lu-Hf ages for eclogites in the Alps are consistently two to six Myr older than U-Pb SHRIMP ages for the same units. For example, the Lu-Hf garnet age of PIS1 is ca. 2 Myr older than the U-Pb SHRIMP age determined for metamorphic zircon in the same sample. This may reflect garnet growth during prograde metamorphism and zircon growth at or after the peak pressure conditions.
- 4) Our tentative paleotectonic model suggests simultaneous subduction of two oceanic basins in the Western Alps.

Acknowledgments

We thank reviewers Jan Kramers and Alfons Berger as well as guest editor Stefan Schmid for their constructive and very helpful criticism. We would also like to thank Klaus Peter Jochum and Brigitte Stoll for supervising the LA-ICP-MS analyses. Work of N.F., T.J.N., and J.P. was supported by DFG project FR700/6. Special thanks goes to Angelika and Thomas Herwartz for their selfless support of my Education.

REFERENCES

Agard, P., Monié, P., Jolivet, L. & Goffé, B. 2002: Exhumation of the Schistes Lustrés complex: in situ laser probe $^{40}\text{Ar}/^{39}\text{Ar}$ constraints and implications for the Western Alps. *Journal of Metamorphic Geology* 20, 599–618.

Albarède, F., Telouk, P., Blichert-Toft, J., Boyet, M., Agranier, A., Nelson, B., 2004: Precise and accurate isotopic measurements using multiple-collector ICPMS. *Geochemica et Cosmochemica Acta* 68, 2725–2744.

Avigad, D., Chopin, C., Goffé, B. & Michard, A. 1993: Tectonic model for the evolution of the Western Alps. *Geology* 21, 659–662.

Becker, H. 1997: Sm-Nd garnet ages and cooling history of high-temperature garnet peridotite massifs and high-pressure granulites from lower Austria. *Contributions to Mineralogy and Petrology* 127, 224–236.

Bill, M., O'Dogherty, L., Guex, J., Baumgartner, P. O. & Masson, H. 2001: Radiolarite ages in Alpine-Mediterranean ophiolites: Constraints on the oceanic spreading and the Tethys-Atlantic connection. *Geological Society of America Bulletin* 113, 129–143.

Bizzarro, M., Baker, J.A., Haack, H., Ulfbeck, D. & Rosing, M. 2003: Early history of Earth's crust-mantle system inferred from hafnium isotopes in chondrites. *Nature* 421, 931–933.

Blichert-Toft J. & Albarède F. 1997: The Lu-Hf isotope geochemistry of chondrites and the evolution of the mantle-crust system. *Earth and Planetary Science Letters* 148, 243–258.

Blichert-Toft, J., Boyet, M., Télouk, P., Albarède, F. 2002: ^{147}Sm - ^{143}Nd and ^{176}Lu - ^{176}Hf in eucrites and the differentiation of the HED parent body. *Earth and Planetary Science Letters* 204, 167–181.

Borghini, A., Compagnoni, R. & Sandrone, R. 1996: Composite P-T paths in the internal Penninic Massifs of the western Alps: Petrological constraints to their thermo-mechanical evolution, *Eclogae geologicae Helvetiae* 89, 345–367.

Bousquet, R., Engi, M., Gosso, G., Oberhänsli, R., Berger, A., Spalla, M.I., Zucali, M. & Goffé, B. 2004: Explanatory notes to the map: Metamorphic structure of the Alps Transition from the Western to the Central Alps. *Mitteilungen der Österreichischen Mineralogischen Gesellschaft* 149, 145–156.

Boynnton, W.V. (1984): Cosmochemistry of the rare earth elements; meteorite studies, in Henderson, P. (Ed.), *Rare Earth Element Geochemistry*, Elsevier, Amsterdam, 1984, pp. 63–102.

Brouwer, F.M., Burri, T., Engi, M., Berger, A. 2005: Eclogite relics in the Central Alps: PT – evolution, Lu-Hf ages and implications for formation of tectonic mélange zones. *Schweizerische Mineralogische und Petrographische Mitteilungen* 85, 147–174.

Bucher, S. 2003: The Briançonnais units along the ECORS-CROP transect (Italian-French Alps): structures, metamorphism and geochronology. Unpublished PhD thesis, University Basel, 175 pp.

Burton, K.W., Kohn, M.J., Cohen A.S. & O'Nions, R.K. 1995: The relative diffusion of Pb, Nd, Sr and O in garnet. *Earth and Planetary Science Letters* 133, 199–211.

Chauvel, C. & Blichert-Toft, J. 2001: A hafnium isotope and trace element perspective on melting of the depleted mantle. *Earth and Planetary Science Letters* 190, 137–151.

Cliff, R.A., Barnicoat, A.C., Inger, S. 1998: Early Tertiary eclogite facies metamorphism in the Monviso Ophiolite. *Journal of Metamorphic Geology* 16, 447–455.

Cohen, A.S., O'Nions, R.K., Siegenthaler, R. & Griffin, W.I. 1988: Chronology of the pressure-temperature history recorded by a granulite terrain. *Contributions to Mineralogy and Petrology* 98, 303–311.

Dal Piaz, G.V., Cortiana, G., Del Moro, A., Martin, S., Pennacchioni, G. & Tartarotti, P. 2001: Tertiary age and paleostructural inferences of the eclogitic imprint in the Austroalpine outliers and Zermatt-Saas ophiolite, western Alps. *International Journal of Earth Sciences* 90, 668–684.

De Capitani C. 1994: Gleichgewichts-Phasendiagramme: Theorie und Software. Beihefte zum *European Journal of Mineralogy* 72. Jahrestagung der Deutschen Mineralogischen Gesellschaft 6, 48.

Dodson, M., H. 1973: Closure Temperature in Cooling Geochronological and Petrological Systems. *Contributions to Mineralogy and Petrology* 40, 259–274.

Duchêne, S., Blichert-Toft, J., Luais, B., Télouk, P., Lardeaux, J.M. & Albarède, F. (1997): The Lu-Hf dating of garnets and the ages of the Alpine high-pressure metamorphism. *Nature* 387, 586–589.

Escher, A., Masson, H. & Steck, A. 1993: Nappe geometry in the western Swiss Alps. *Journal of Structural Geology* 15, 501–509.

Frisch, W. 1979: Tectonic progradation and plate tectonic evolution of the Alps. *Tectonophysics* 60(3–4), 121–139.

Froitzheim, N. & Manatschal, G. 1996: Kinematics of Jurassic rifting, mantle exhumation, and passive-margin formation in the Austroalpine and Penninic nappes (eastern Switzerland). *Geological Society of America Bulletin* 108, 1120–1133.

Froitzheim, N., Schmid, S.M. & Frey, M. 1996: Mesozoic paleogeography and the timing of eclogite facies metamorphism in the Alps: A working hypothesis. *Eclogae geologicae Helvetiae* 89(1), 81–110.

- Froitzheim, N. 2001: Origin of the Monte Rosa nappe in the Pennine Alps: A new working hypothesis. *Geological Society of America Bulletin* 113, 604–614.
- Froitzheim, N., Pleuger, J., Roller, S. & Nagel, T. 2003: Exhumation of high- and ultrahigh-pressure metamorphic rocks by slab extraction. *Geology*, 31, 925–928.
- Gebauer, D. 1996: A P–T–t path for an (ultra?) high-pressure ultramafic/ mafic rock-association and its felsic country-rocks based on SHRIMP-dating of magmatic and metamorphic zircon domains. Example: Alpe Arami (Central Swiss Alps). In: Basu, A., Hart, S. (Eds.), *Earth Processes: Reading the Isotopic Code*. Geophys. Monogr. AGU. Washington DC 95, 307–329.
- Gebauer, D., Schertl, H.P., Brix, M. & Schreyer, W. 1997: 35 Ma old ultrahigh-pressure metamorphism and evidence for very rapid exhumation in the Dora Maira massif, Western Alps. *Lithos* 41, 5–24.
- Hensen, B.J. & Zhou, B. 1995: A Pan-African granulite facies metamorphic episode in Prydz Bay, Antarctica: evidence from Sm–Nd garnet dating. *Australian Journal of Earth Science* 42(3), 249–258.
- Hofmann, A.W. 1988: Chemical differentiation of the Earth: the relationship between mantle, continental crust and oceanic crust. *Earth and Planetary Science Letters* 90, 297–314.
- Inger, R., Ramsbotham, W., Cliff, R.A. & Rex, D.C. 1996: Metamorphic evolution of the Sesia-Lanzo Zone, Western Alps: time constraints from multi-system geochronology. *Contributions to Mineralogy and Petrology* 126, 152–168.
- Jacobsen, S.B., Wasserburg, G.J. 1980: Sm–Nd isotopic evolution of chondrites. *Earth and Planetary Science Letters* 50, 139–155.
- Jagoutz, E. 1988: Nd and Sr systematics in an eclogite xenolith from Tanzania: Evidence for frozen mineral equilibria in the continental lithosphere. *Geochimica et Cosmochimica Acta* 52, 1285–1293.
- Jochum K.P., Stoll B., Herwig K. & Willbold M. 2007: Validation of LA-ICP-MS trace element analysis of geological glasses using a new solid-state 193 nm Nd: YAG laser and matrix-matched calibration. *Journal of Analytical Atomic Spectrometry* 22(2), 112–121.
- John, T., Schere, E.E., Haase, K. & Schenk, V. 2004: Trace element fractionation during fluid-induced eclogitization in a subduction slab: trace element and Lu–Hf–Sm–Nd isotope systematics. *Earth and Planetary Science Letters* 277, 441–456.
- Kaczmarek, M.A., Müntener, O. & Rubatto, D. 2008: Trace element chemistry and U–Pb dating of zircons from oceanic gabbros and their relationship with whole rock composition (Lanzo, Italian Alps). *Contributions to Mineralogy and Petrology* 155, 295–312.
- Keller, L.M. & Schmid, S.M. 2001: On the kinematics of shearing near the top of the Monte Rosa nappe and the nature of the Furgg zone in Val Loranco (Antrona valley, N. Italy): Tectonometamorphic and paleogeographical consequences. *Schweizerische Mineralogische und Petrographische Mitteilungen* 81, 347–367.
- Kohn, M.J. 2003: Geochemical zoning in metamorphic minerals. In: Rudnik, R.L. (Ed.), *The Crust. Treatise on Geochemistry* 3, 229–261.
- Kramer J., Abart, R., Müntener, O., Schmid, S.M., Stern, W. 2003: Geochemistry of metabasalts from ophiolitic and adjacent distal continental margin units: Evidence from the Monte Rosa region (Swiss and Italian Alps). *Schweizerische Mineralogische und Petrographische Mitteilungen* 83, 217–240.
- Kretz, R. 1983: Symbols for rock-forming minerals. *American Mineralogist* 68, 277–279.
- Lagos, M., Scherer, E.E., Tomaschek, F., Münker, C., Keiter, M., Berndt, J., Ballhaus, C. 2007: High precision Lu–Hf geochronology of Eocene eclogite-facies rocks from Syros, Cyclades, Greece. *Chemical Geology* 243, 16–35.
- Lapen, T.J., Johnson, C.M., Baumgartner, L.P., Mahlen, N.J., Beard, B.L. & Amato, J.M. 2003: Burial rates during prograde metamorphism of an ultrahigh-pressure terrane: an example from Lago di Cignana, Western Alps, Italy. *Earth and Planetary Science Letters* 215, 57–72.
- Lapen, T.J., Johnson, C.M., Baumgartner, L.P., Dal Piaz, G.V., Skora, S. & Beard, B.L. 2007: Coupling of oceanic and continental crust during Eocene eclogite facies metamorphism: evidence from the Monte Rosa nappe, western Alps. *Contributions to Mineralogy and Petrology* 153, 139–157.
- Liati, A., Gebauer, D. & Fanning, M.C. 2003: The youngest basic oceanic magmatism in the Alps (Late Cretaceous; Chiavenna unit, Central Alps): geochronological constraints and geodynamic significance. *Contributions to Mineralogy and Petrology* 146(2), 144–158.
- Liati, A., Froitzheim, N. & Fanning, C.M. 2005: Jurassic Ophiolites within the Valais domain of the western and central Alps: Geochronological evidence for re-rifting of oceanic crust, *Contributions to Mineralogy and Petrology* 149(4), 446–461.
- Liati, A. & Froitzheim, N. 2006: Assessing the Valais ocean, Western Alps: U–Pb SHRIMP zircon geochronology of eclogite in the Balma unit, on top of the Monte Rosa nappe. *European Journal of Mineralogy* 18(3), 299–308.
- Ludwig, K.R. 2001: Isoplot/Ex version 2.49, Geochronological Toolkit for Microsoft Excel, Berkeley Geochronology Center Special Publications 1a.
- Mahlen, N.J., Lapen, T.J., Johnson, C.M., Baumgartner, L.P. & Beard, B.L. 2003: Duration of Prograde Metamorphism as constrained by high-precision Lu–Hf Geochronology of HP/UHP Eclogites from the western Alps. *Geological Society of America Abstracts with Programs* 35(6), 638.
- Mahlen, N.J., Skora, S., Johnson, C.M., Baumgartner, L.P., Lapen, T.J., Beard, B.L. & Pilet, S. 2005: Lu–Hf geochronology of eclogites from Pfulwe, Zermatt-Saas Ophiolite, western Alps, Switzerland. *Geochimica et Cosmochimica Acta* 69, A305–A305 Suppl. S.
- Mahlen, N.J., Johnson, C.M., Baumgartner, L.P., Lapen, T.J., Skora, S. & Beard, B.L. 2006: Protracted Subduction History and HP/UHP Metamorphism of the Zermatt-Saas-Ophiolite, Western Alps, as Constrained by Lu–Hf Geochronology. *Eos Trans. AGU* 87 (52), Fall Meeting Supplement.
- McDounough, W.F., & Sun, S. s. 1995: The composition of the Earth. *Chemical Geology* 120, 223–253.
- Mezger, K., Essene, E.J. & Halliday, A.N. 1992: Closure temperatures of the Sm–Nd system in metamorphic garnets. *Earth and Planetary Science Letters* 113, 397–409.
- Münker C., Weyer S., Scherer E. & Mezger K. 2001: Separation of high field strength elements (Nb, Ta, Zr, Hf) and Lu from rock samples for MC-ICPMS measurements. *Geochemistry Geophysics Geosystems* 2, Nr. 2001GC000183
- Oberli, F., Meier, M., Berger, A., Rosenberg, C.L., Gieré, R. 2004: U–Th–Pb and $^{230}\text{Th}/^{238}\text{U}$ disequilibrium isotope systematics: Precise accessory mineral chronology and melt evolution tracing in the Alpine Bergell intrusion. *Geochimica et Cosmochimica Acta*, 68 (11), 2543–2560.
- Patchett, P.J. & Tatsumoto, M. 1980: A routine high precision method for Lu–Hf isotope geochemistry and chronology. *Contributions to Mineralogy and Petrology* 75, 263–267.
- Pleuger, J., Froitzheim, N. & Jansen, E. 2005: Folded continental and oceanic nappes on the southern side of Monte Rosa (Western Alps, Italy): anatomy of a double collision suture. *Tectonics* 24, DOI 10.1029/2004TC001737
- Pleuger, J., Roller, S., Walter, J.M., Jansen, E. & Froitzheim, N. 2007: Structural evolution of the contact between two Penninic nappes (Zermatt-Saas zone and Combin zone, Western Alps) and implications for the exhumation mechanism and palaeogeography. *International Journal of Earth Science* 96, 229–252.
- Ravna, E.J.K. & Terry, M.P. 2004: Geothermobarometry of UHP and HP eclogites and schists – an evaluation of equilibria among garnet-clinopyroxene-kyanite-phengite-coesite/quartz. *Journal of Metamorphic Geology* 22(6), 579–592.
- Reinecke, T. 1991: Very-high-pressure metamorphism and uplift of coesite-bearing metasediments from the Zermatt-Saas zone, Western Alps. *European Journal of Mineralogy* 3, 7–17.
- Reinecke, T. 1998: Prograde high- to ultrahigh-pressure metamorphism and exhumation of oceanic sediments at Lago di Cignana, Zermatt-Saas Zone, western Alps. *Lithos* 42, 147–189.
- Richard, P., Shimizu, N., Allègre, C.J. 1976: $^{143}\text{Nd}/^{144}\text{Nd}$ a natural tracer: An application to oceanic basalts. *Earth and Planetary Science Letters* 31, 269–278.
- Rubatto, D., Gebauer, D. & Fanning, M. 1998: Jurassic formation and Eocene subduction of the Zermatt-Saas Fee Ophiolites: implications for the geodynamic evolution of the central and western Alps. *Contributions to Mineralogy and Petrology* 132, 269–287.
- Rubatto, D. & Gebauer, D. 1999: Eocene/Oligocene (35 Ma) high-pressure metamorphism in the Gornergrat Zone (Monte Rosa, Western Alps):

- Implications for paleogeography. *Schweizerische Mineralogische und Petrographische Mitteilungen* 79, 353–362.
- Rubatto, D., Gebauer, D. & Compagnoni, R. 1999: Dating of eclogite-facies zircons: The age of Alpine metamorphism in the Sesia-Lanzo zone (western Alps). *Earth and Planetary Science Letters* 167, 141–158.
- Rubatto, D. & Hermann, J. 2001: Exhumation as fast as subduction? *Geology* 29, 3–6.
- Rubatto, D. & Hermann, J. 2003: Zircon formation during fluid circulation in eclogites (Monviso, Western Alps): implications for Zr and Hf budget in subduction zones. *Geochimica et Cosmochimica Acta* 67, 2173–2187.
- Salters, V.J.M. & White, W.M. 1998: Hf isotope constraints on mantle evolution. *Chemical Geology* 145, 447–460.
- Scherer, E., Cameron, K.L. & Blichert-Toft, J. 2000: Lu–Hf garnet geochronology: Closure temperature relative to the Sm–Nd system and the effects of trace mineral inclusions. *Geochimica et Cosmochimica Acta* 64 (19), 3413–3432.
- Scherer, E., Münker, C. & Mezger, K. 2001: Calibration of the Lutetium–Hafnium Clock. *Science* 293, 683–687.
- Schmid, S.M., Pfiffner, O.A., Froitzheim, N., Schönborn, G. & Kissling, E. 1996: Geophysical-geological transect and tectonic evolution of the Swiss-Italian Alps. *Tectonics* 15, 1036–1064.
- Schmid, S.M., Fügenschuh, B., Kissling, E. & Schuster, R. 2004: Tectonic map and overall architecture of the Alpine orogen. *Eclogae geologicae Helveticae* 97(1), 93–117.
- Skora, S., Baumgartner, L.P., Mahlen, N.J., Johnson, C.M., Pilet, S. & Hellbrand, E. 2006: Diffusion-limited REE uptake by eclogite garnets and its consequences for Lu–Hf and Sm–Nd geochronology. *Contributions to Mineralogy and Petrology* 152, 703–720.
- Skora, S., Baumgartner, L.P., Mahlen, N.J., Lapen, T.J., & Johnson, C.M. 2006b: Lu/Hf closure temperature estimated from alpine eclogite garnets. 4th Swiss Geoscience Meeting, Bern 2006.
- Söderlund, U., Patchett, P.J., Vervoort, J.D., and Isachsen, C.E. 2004: The ¹⁷⁶Lu decay constant determined by Lu–Hf and U–Pb isotope systematics of Precambrian mafic intrusions. *Earth and Planetary Science Letters* 219, 311–324.
- Spear, F.S. 1991: On the interpretation of peak metamorphic temperatures in light of garnet diffusion during cooling. *Journal of Metamorphic Geology* 9(4), 379–388.
- Stampfli, G.M. 1993: Le Briançonnais, terrain exotique dans les Alpes? *Eclogae geologicae Helveticae* 86, 1–45.
- Stampfli, G.M., Mosar, J., Marquer, D., Marchant, R., Baudin, T. & Borel, G. 1998: Subduction and obduction processes in the Swiss Alps. *Tectonophysics* 296, 159–204.
- Stampfli, G.M. & Borel, G.D. 2004: The TRANSMED transects in space and time: Constraints on the paleotectonic evolution of the Mediterranean domain. In: Cavazza, W., Roure, F.M., Spakman, W., Stampfli, G.M. & Ziegler, P.A. (Eds.) *The TRANSMED Atlas*. Springer, Berlin Heidelberg, 53–80.
- Steck, A., Biggoggero, B., Dal Piaz, G.V., Escher, A., Martinotti, G. & Masson, H. 1999: Carte tectonique des Alpes de Suisse occidentale et des régions avoisinantes, 1:100'000, Carte spéc. n. 123 (4 maps). *Serv. hydrol. géol. nat.*, Bern
- Thoeni, M. (2002): Sm–Nd isotope systematics in garnet from different lithologies (Eastern Alps); age results, and an evaluation of potential problems for garnet Sm–Nd. *Chemical Geology* 185 (3–4), 255–281.
- Tirone, M., Ganguly, J., Dohmen, R., Langenhorst, F., Hervig, R. & Becker, H.W. 2004: Rare earth diffusion kinetics in garnet: Experimental studies and applications. *Geochimica et Cosmochimica Acta* 69(9), 2385–2398.
- Van Orman, J.A., Grove, T.L., Shimizu, N. & Graham, D.L. 2002a: Rare earth element diffusion in a natural pyrope single crystal at 2.8 GPa. *Contributions to Mineralogy and Petrology* 142, 416–424.
- Vervoort, J.D., Patchett, P.J., Söderlund, U., Baker, M. 2004: The isotopic composition of Yb and the determination of Lu concentrations and Lu/Hf ratios by isotope dilution using MCICPMS. *Geochemistry Geophysics Geosystems* 5 (11), doi:10.1029/2004GC000721.

Manuscript received March 3, 2008

Revision accepted June 6, 2008

Published Online first November 8, 2008

Editorial Handling: Stefan Schmid & Stefan Bucher